Nano Energy 87 (2021) 106162

Contents lists available at ScienceDirect

Nano Energy

journal homepage: www.elsevier.com/locate/nanoen

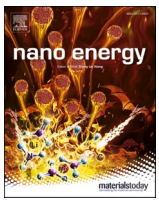

Review

The promise of hydrogen production from alkaline anion exchange membrane electrolyzers

Changqing Li, Jong-Beom Baek *

School of Energy and Chemical Engineering, Center for Dimension-Controllable Organic Frameworks, Ulsan National Institute of Science and Technology (UNIST), 50 UNIST, Ulsan 44919, South Korea

ARTICLE INFO

Keywords:
Anion exchange membrane
Electrolyzer
Ionomer
Platinum group metal-free catalyst
Hydrogen production

ABSTRACT

Producing hydrogen using anion exchange membrane (AEM) water electrolysis is a promising approach to address the severe energy crisis facing human society. AEM electrolysis can be integrated with intermittent and sustainable energy sources, utilize low-cost electrocatalysts and other inexpensive components in stacks. The sporadic investigation on catalysts and membrane development of AEM electrolysis enable it still under the early stage of development. To enable commercially viable hydrogen generation, deeper understanding and improvement of AEM electrolysis technology is imperative, including power efficiency, stack feasibility, membrane stability, ion conductivity, robustness and cost reduction. In this review, the basic principles, progress and challenges of AEM are discussed. We highlight recent achievements in electrocatalysts, alkaline exchange membranes, ionomers, and the resulting AEM electrolyser performance. In particular, development challenges facing AEM electrolysis are summarized. Hopefully, this review paper will attract additional interest to close technical gaps, while providing practical research recommendations for AEM electrolysis research, leading to scalable hydrogen production.

1. Introduction

Sustainable and clean energy conversion and storage technologies are considered the most important approaches among emerging efforts to address the severe global energy crisis and environmental issues facing modern society [1–7]. A variety of energy-related devices, including fuel cells, solar cells, lithium-ion batteries, supercapacitors and water electrolyzers are currently in development [8–15]. In the energy conversion field, water electrolysis is particularly promising, since it can utilize intermittent clean energy sources, such as wind, tides and solar energy, to produce hydrogen from unlimited water resources. Hydrogen as an ideal energy carrier, and advanced electrolysis systems are expected to be a superior hydrogen acquisition method, compared with traditional hydrocarbon extraction [16–22].

Hydrogen can be produced from water molecules using a variety of approaches, such as water splitting and electrolysis [23–27]. Traditional water splitting methods usually involve a thermochemical reforming process and the chemical conversion of biomass to produce hydrogen and oxygen gases. These complex and consecutive chemical reactions are typically driven by metal-based catalysts [28–30]. This conversion process requires rather high reaction temperatures (800–2000 °C), and the heat is commonly supplied from solar or nuclear power plants [31,32]. Although this thermochemical method has some distinct advantages, issues remain with separating components at various stages.

Producing hydrogen by photoelectrocatalytic water splitting is also promising, and the technology conventionally relies on TiO_2 photocatalysts [33]. TiO_2 has an intrinsic wide band gap in the visible light region, and this enables it to produce a high overpotential during photocatalysis, which can be further optimized by modifying the electron-hole pairs [34]. A number of measures are employed to address TiO_2 shortcomings, for example, by synergistically coupling with carbon materials [35], modifying with adsorbents [36], or down-scaling the TiO_2 into nano-size particles [37]. Graphitic carbon nitride (g-C_3N_4), with its distinct semiconductor property and low-cost characteristics, has also been explored and used for efficient photocatalytic H_2 production [38]. In a further improvement, effective methods to control the band structure of g-C_3N_4 have been developed, by metal doping, interaction with carbon hybrid, and by introducing heterojunctions at the interface, resulting in superior photocatalytic performance [39,40].

Water electrolysis is a well-established technique for converting

* Corresponding author.
E-mail address: jbbaek@unist.ac.kr (J.-B. Baek).

https://doi.org/10.1016/j.nanoen.2021.106162
Received 8 February 2021; Received in revised form 8 May 2021; Accepted 12 May 2021
Available online 18 May 2021

water into molecular hydrogen and oxygen at relatively low temperatures. The ever-increasing demand for sustainable energy carriers has rekindled interest in efficient and flexible methods of acquiring high-quality hydrogen (~100% hydrogen) [41–44].

Modern water electrolysis systems can be divided into proton exchange membrane (PEM) electrolysis and alkaline water electrolysis, based on the type of electrolyte.

1.1. PEM electrolysis

The first PEM electrolysis cell based on a solid polymer electrolyte concept was reported by Russell et al. and the Genetic Electric corporation in 1973 [45]. The concept was further enhanced and later named proton exchange membrane or polymer electrolyte membrane (PEM) water electrolysis by Grubb [46,47]. The PEM electrolyser uses noble metal-based materials such as IrO_2 for the anode and Pt black as the cathode catalysts (Fig. 1a). An acidic polymer membrane (Nafion@ or fumapem@) is employed as the electrolyte to ensure high proton conductivity, and to prevent hydrogen and oxygen gas crossover in the reaction chamber. This enables a compact system design and the possibility of high-pressure working conditions. The kinetics for producing hydrogen using PEM electrolysis are better than in alkaline electrolysis, given the readily available protons on the surface of the metal catalyst. Nevertheless, PEM electrolysis suffers from the high price of Nafion-based membranes. The cation impurities released from feed water in the cathode chamber and the components of electrolysis units will occupy the ion exchange sites of Nafion polymer electrolyte in the catalyst layers and membrane, resulting in a degradation of PEM electrolyzer during long-term operation [48–50]. More importantly, the stack materials used for the configuration of PEM system are more expensive than those used for alkaline electrolysis [51].

1.2. Alkaline water electrolysis

Alkaline electrolysis employs two non-platinum group metal (Ni and Fe) based electrodes, a diaphragm membrane and 30–40% KOH electrolyte (Fig. 1b). Alkaline electrolysis is regarded a reliable technology for producing hydrogen up to the megawatt scale [52]. The circulating KOH electrolyte provides the necessary alkalinity. A porous diaphragm serves as the separator to uncouple the anode and cathode. It also serves the vital function of conducting hydroxyl ions, and preventing possible gas crossover, ensuring efficiency and safety [53,54]. The diaphragm is made of ceramic oxide materials, such as asbestos and potassium titanate, or an organic polymer such as polypropylene [55–60]. Among its advantages, alkaline water electrolysis can use non-noble metal catalysts and provides easily handling flexibility because of its relatively low temperature operating condition [61]. Some specific characteristics of the alkaline water electrolyzer are listed in Table 1.

Alkaline electrolyzers also have three major drawbacks, a low partial load range, low maximum achievable current density and the inability to operate at high pressure. In practice, the diaphragm cannot completely prevent produced gas crossover over the anode and cathode chamber. Oxygen diffused into the cathode chamber will react with hydrogen produced on the cathode side, and hydrogen diffusion into the oxygen evolution chamber can even pose a critical safety problem, considering the low explosion limit of hydrogen (>4 mol% H_2) [62].

Another knotty issue is the system's low current density, which results from the high impedance of the liquid electrolyte and diaphragm. A third problem is related to the electrolyte property. The liquid inhibits alkaline electrolyzers at higher pressure, thus requiring a bulky stack configuration. Additionally, the oxygen produced from the anode will inevitably contact CO_2 in the air, leading to the formation of K_2CO_3 in the system [63,64]. This degrades electrocatalytic performance, because: 1) the reaction process between CO_2 and KOH consumes many of the hydroxyl ions needed for oxygen evolution; 2) the ionic

Table 1
Comparison of alkaline, PEM and AEM electrolysis.

	Alkaline	PEM	AEM
Electrolyte	20–30% KOH	Perfluorosulfonic acid	Quaternary ammonia polysulfone or optional dilute caustic solution
Operating temperature (°C)	65–100	70–90	50–70
OER/HER catalysts	Ni/Fe based species	Platinum groups	Ni based materials
Current collector materials	Ni plate	Titanium plate	Ni plate
Available current density (mA cm^{-2})	200–500	800–2300	100–500
Investigated durability (h)	100,000	< 5000	Not available
Production yield (N m^3 h^{-1})	100–760	~30	2.05–1
Hydrogen content (vol%)	9.99–99.3	99.9999	99.99
Estimated cost (€ kg-1)	800–1300	> 1200	Not available
Developing status	Mature technology	Mature for small scale	Under developing

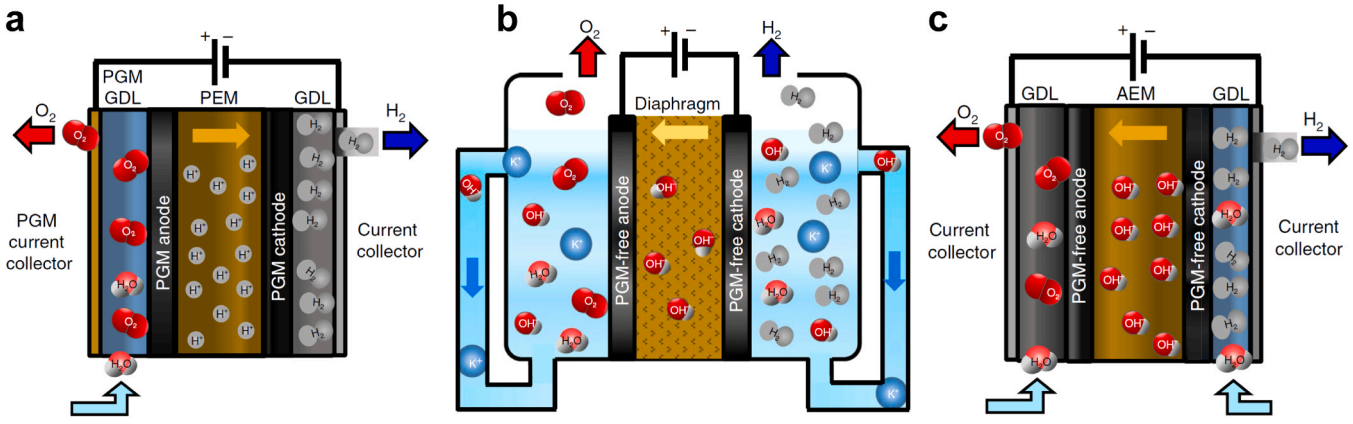

Fig. 1. Schematic diagram of PEM and AEM electrolysis cells. a, PEM electrolyser based PGM-based cathode (Pt) and anode (IrO_2). b, Alkaline water electrolyzer with KOH electrolyte circulating in the reaction chamber, Ni and/or Fe based PGM-free materials as electrode. c, AEM electrolyser using Ni based electrode and Ti plate current collectors. PGM: platinum group metal; GDL: gas diffusion layer.
Reproduced with permission [139]. Copyright 2020, Nature Publishing Group.

conductivity is reduced because of changes in electrolyte composition; 3) the K_2CO_3 precipitate is adsorbed on the pores of the gas diffusion layer (GDL), diminishing the ion transfer rate [65–67].

1.3. Anion exchange membrane (AEM) electrolysis

AEM water electrolysis cells consist of a hydrocarbon anion exchange membrane and two transition metal catalyst-based electrodes. The distilled water or a low concentration alkaline solution can be utilized as the electrolyte in the AEM, rather than concentrated KOH solution (Fig. 1c). The AEM approach combines the merits of PEM and alkaline electrolysis [68–70]. Polymeric anion exchange membranes have recently been developed by researchers from organizations and universities, although interest has predominantly been focused on catalyst design towards half-cell test rather than the further application of AEM electrolysis.

Complete studies on AEM water electrolysis are rare when searching the keywords "anion exchange membrane water electrolysis" on the Web of Science site, which suggests that AEM electrolysis technology is still under early development and requires further investigation. Coordinated research of AEM electrolysis is currently needed to improve power efficiency, membrane stability and ionic conductivity, to reduce the total stack cost, and to integrate catalysts into AEM systems. Some works that have been conducted at laboratory scale provide valuable guidance for understanding the operating mechanism [71–73], and developing the main electrocatalyst [74–76], membrane and ionomer components [77,78]. The crucial AEM materials (catalysts, membranes, and ionomers) and operating conditions (electrolyte, applied voltage, available current density, and operating temperature) are summarized in Table 2 for systematic comparison.

2. Main AEM components

One of the predominant benefits of AEM electrolysis is the ability to use platinum group metal (PGM)-free electrocatalysts towards the hydrogen evolution reaction (HER) and oxygen evolution reaction (OER) in separate reaction chambers. This reduces the capital cost of AEM water electrolysis. Current challenges in AEM catalyst development are the optimization of chemical composition, stability and overall activity when integrated in the AEM system [43,79,80]. PGM-free electrocatalysts usually have relatively low mass-specific activity compared with noble metal-based catalysts, which leads to large catalyst loading on the membrane electrode assembly (MEA) and large Ohmic resistance losses.

2.1. HER catalysts

Noble metal Ruthenium and Iridium (Pt, Ru and Ir) based HER catalysts have demonstrated excellent HER activity in a pH-universal environment [81–83]. PGM-free HER electrocatalysts lack this property, because HER kinetics are sluggish under alkaline conditions, due to the further proton dissociation step from water molecules and the formation of hydrogen intermediates (H_{ad}) on comparing with catalyst working in acid condition [84].

The alkaline HER involves three reaction steps [85]:

$$\text{The Volmer step: } H_2O + e^- + \text{catalyst} = \text{catalyst-}H_{ad} + OH^- \quad (1)$$

$$\text{followed by the Heyrovsky step: } H_2O+\text{catalyst-Had}+e^- = \text{catalyst}+H_2+OH^- \quad (2)$$

$$\text{or the combined Tafel step: } 2\text{catalyst-}H_{ad} = \text{catalyst} + H_2 \quad (3)$$

As originally reported by Parsons, H_2O dissociation and subsequent H_{ad} adsorption on the catalyst surface is quite slow and hence the formation of initial hydrogen intermediates becomes the rate determining step (RDS) of the entire HER mechanism [86]. This makes the alkaline

Table 2
Brief comparison of components, operating parameters and cell performance of AEM electrolysis.

Electrolyte	Membrane electrode assembly (MEA)								Operating parameters			References
	Cathode			Anode			AEM membrane	Ionomers				
	GDL	Catalysts	Loading (mg cm^{-2})	GDL	Catalysts	Loading (mg cm^{-2})			Applied voltage (V)	Current density (mA cm^{-2})	Operating temperature (°C)	
KOH	Titanium	NiMo alloy	5	Titanium	Ir black	3	FAA 3-PE	FAA-3-SOLUT-10	1.9	1000	50	[79]
1% K_2CO_3	Carbon paper	Ni/(CeO_2-La_2O_3)/C	7.4	Ni foam	CuCoOx	30	A201	I_2, Acta Spa, Italy	1.95	500	60	[180]
1 M KOH	Ni foam	Co_3S_4	3	Ni foam	$Cu_{0.81}Co_{2.19}O_4$ NS	4	X37–50	–	2.0	431	45	[181]
10% KOH	Ni foam	$NiCo_2O_4$	10	Ni foam	Ni foam	–	–	qPPO	1.85	135	50	[160]
Pure water	Carbon paper	Pt/C	3	Titanium	IrO_x	3	FAA-3	FAA-3	2.29	500	50	[104]
1 M KOH	Carbon paper	Pt/C	1.3	Carbon paper	NiFe-LDH	2.5	X37–50	Nafion	1.59	1000	80	[103]
1 M KOH	Carbon	Pt/C	0.4	Titanium	IrO_2	4	FAA-3–50	FAA-3-Br	1.9	1500	70	[156]
10% K_2CO_3	Ni foam	Pt	1.7	Ni foam	$CuCoO_x$	4.1	A201	AS-4	1.91	1000	50	[165]
1 M NaOH	SGL 29 BCE	Ni_9Mo_1/C	2	platinized titanium	Ni_2Fe_1	3	HTMA-DAPP	TMA	1.8	906	60	[139]
0.1 M NaOH	Carbon cloth	$CuCoO_3$	40	Ni foam	Ni/(CeO_2-La_2O_3)/C	40	Mg-Al LDH	PTFE	2.2	208	70	[146]

HER more complex than HER in acidic conditions, because some important species/steps (H_{ad}, hydroxyl adsorption and water dissociation) must be optimized for superior performance [87,88]. Specifically, in AEM HER electrolysis more energy is required to break the robust H-O covalent bonds of water, and is regarded a crucial step that determines HER activity [89]. Within this context, rational design of PGM-free HER electrocatalysts on AEM system is of superb importance to bring out the distinguished advantages over the PEM for up-coming hydrogen society. Some studies have also reported the superior performance of AEM eletrolyzer using PGM-free HER catalyst over the PGM-based materials in either PEM and AEM system. Their application further proves the reliable hydrogen acquisition in the AEM approach. Here, the development of those inexpensive HER materials evaluated in AEM electrolysis is emphasized in this section.

Ni based hybrids are frequently adopted as HER catalysts in AEM electrolysis. In most studies, they are reported to have activity inferior to PGM materials. Ni nano-powders with a catalyst loading of 2 mg cm^{-2} can be used as a hydrogen evolution catalyst in AEM electrolysis systems, and have achieved a current density of 100 mA cm^{-2} at an applied voltage of 1.99 V at a temperature of 44 °C [90]. Particle-type electrodes were also developed with ultra-low Ni/Pt particle loading (13.2 μg cm^{-2}), coated on carbon paper. The as-prepared MEA using Pt-Ni/CP-2 as the cathode electrocatalyst exhibited pronounced performance with an available current density of 250 mA cm^{-2} at 1.9 V_{cell} (60 °C). This performance surpassed or approached the top activity in previous reports using a much higher catalyst loading range of 3.1–80 mg cm^{-2} [91]. Despite this, Ni metal still has relatively poor activity and stability, and for enhanced performance needs to be combined with other materials, such as transition metals-based oxides, chalcogenide selenides, nitrides and phosphides [92].

Using commercially available materials such as ACTA 3030 (Ni/(CeO_2-La_2O_3)/C) as the HER electrocatalyst, the performance of these mixed Ni base oxides was tested in a diluted K_2CO_3/$KHCO_3$ electrolyte solution (pH 10–11) separated by an A-201 anion exchange membrane (Tokuyama Corporation) [93]. The catalyst loading on the cathode was thought to have a huge influence on the performance of the AEM system when the $CuCoO_x$ mixed oxides was fixed at the loading of 36 mg cm^{-2} on anode. By varying the Ni/(CeO_2-La_2O_3)/C loading from 0.6 to 7.4 mg cm^{-2}, an exported cell potential between 2.01 and 1.89 V was obtained at 470 mA cm^{-2} at 43 °C. The cathode catalyst loading also affected the alternating-current (AC/1 kHz) resistance at different current density values, although the reaction mechanism remains controversial in light of complexity of the system. It is also worth noting that stability of the as-prepared system was remarkable, with no cell potential degradation in 800 h under a constant differential pressure of 3 MPa. This suggests its potential value for durable and efficient hydrogen production.

Employing alloys is also a viable approach to improve HER activity on Ni [94]. A NiMo alloy cathode and NiFe alloy anode were assembled and impregnated with a self-crosslinking quaternary ammonia polysulfone (xQAPS) membrane as the MEA [95]. The anode and cathode had a high catalyst loading of 40 mg cm^{-2}, which led to an AEM cell performance of 400 mA cm^{-2} at a cell voltage of 1.8–1.85 V under 70 °C pure water electrolyte. In another work, $Ni_{0.9}Mo_{0.1}$ nanosheets were synthesized and tested to have a cathode performance comparable to Pt nanoparticles in a AEM cell [79]. The sponge-like structure of the NiMo alloy was believed to expose a much higher specific surface area. The NiMo/X72 achieved 1 A cm^{-2} at 1.9 V in 1 M KOH, while the Pt particle reached the same current density value at 1.8 V, suggesting a small performance gap between the NiMo alloy and Pt-PGM catalyst (Fig. 2).

The HER electrocatalysts towards AEM in the abovementioned works are simply Ni particles, Ni-based species and Ni-incorporated carbon materials [96]. Research on the design of HER electrocatalysts for AEM is still limited, even though remarkable HER activity has been demonstrated by many PGM-free catalysts in half-cell components [97]. While the NiMo alloy currently holds the outstanding cathode performance in AEM electrolyser cells, the ultimate level of AEM performance is still unknown. Considerable effort is still needed to engineer HER catalysts for practical application and operation.

2.2. OER catalysts

The OER process in alkaline conditions involves the consumption of OH^- anions in multiple steps as the following equation suggests, where M indicates the active catalyst [98]:

$$M + OH^- = MOH + e^- \quad (4)$$

$$MOH + OH^- = MO + H_2O\ (l) + e^- \quad (5)$$

$$MO + OH^- = MOOH + e^- \quad (6)$$

$$MOOH + OH^- = M + O_2\ (g) + H_2O\ (l) + e^- \quad (7)$$

$$\text{Overall: } 4OH^- = O_2\ (g) + 2H_2O\ (l) + 4e^- \quad (8)$$

The multiple four-electron reaction on OER indicates a more complex mechanism and inherently sluggish character compared with HER.

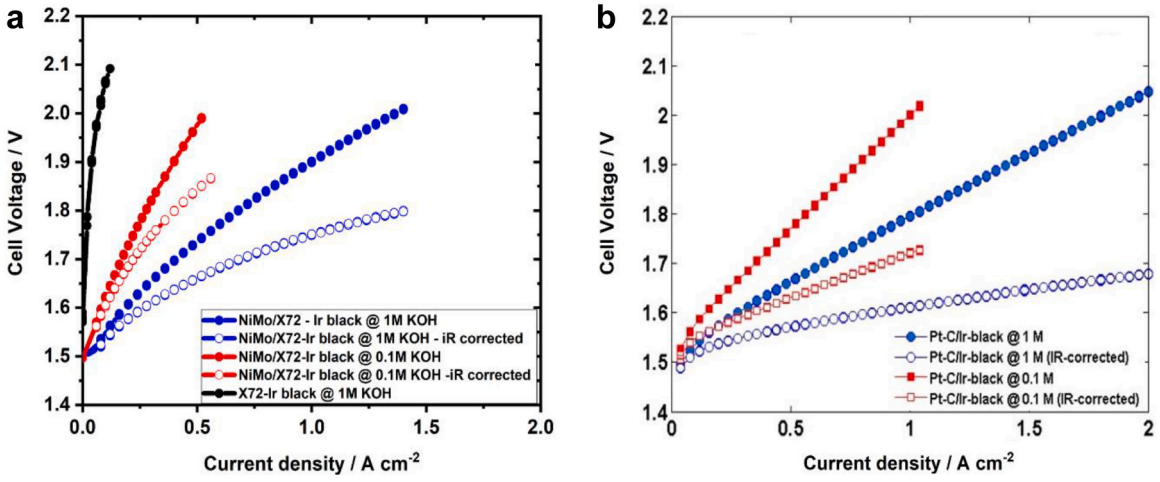

Fig. 2. Current density-voltage polarization curves recorded for different electrolytes (1 M and 0.1 M KOH solution) and electrocatalyst types (NiMo alloy/Ir and Pt/C/Ir PGM-based materials) at 50 °C. (a) NiMo alloy with a catalyst loading of 5 mg cm^{-2}; (b) Pt nanoparticles loaded on a porous carbon matrix at 1 mg cm^{-2} content. Both anode electrodes used 3 mg cm^{-2} of Ir-black.
Reproduced with permission [79]. Copyright 2018, Multidisciplinary Digital Publishing Institute.

It requires efficient catalyst participation to adsorb the reactants and to transfer them as intermediates to the surface of the catalyst for subsequent steps. In an AEM system, cell performance has a close relationship with, and largely depends on, OER.

In contrast with the few works on cathode HER catalysts, many PGM-free electrocatalysts have been explored and tested in integrated AEM cells with excellent performance. Nickel/iron (NiFe)-based materials have been validated with predominant OER activity for multiple applications [99,100]. Their activities are also being evaluated in AEM cells. In a control experiment with atomic ratios (Fe/Ni), a $NiFeO_x$ hybrid was synthesized, and converted from a less crystalline feature to the spinel phase with higher Fe content. When assessed in a single AEM cell, the Ni_1Fe_1 oxide anode showed a large current density of 650 mA cm^{-2} at 2 V below a temperature of 50 °C [101]. However, it had poor durability in a 500 h potential cycling test, losing more than 150 mA cm^{-2} during the initial 400 h.

NiFe-based layered double hydroxides (LDHs), known to be excellent OER catalysts and to accelerate the reaction, have also been studied

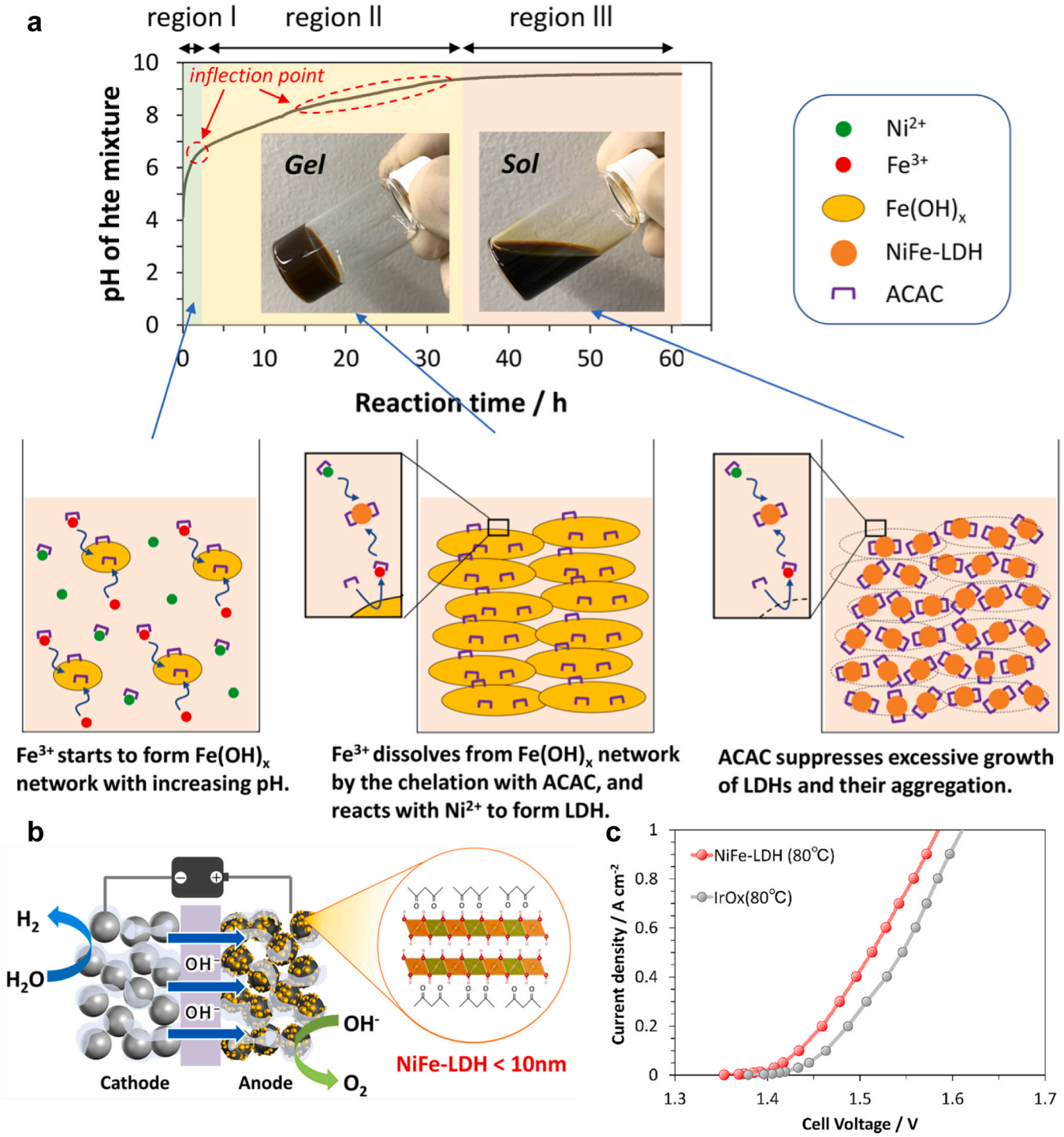

Fig. 3. (a, b) Schematic illustration of NiFe-LDH synthesis mechanism and its application in AEM cells. (c) Polarization curves of membrane electrode assembly (MEA) using NiFe-LDH and IrO_x as the anode catalysts.
Reproduced with permission [103]. Copyright 2020, American Chemical Society.

[102]. A particle lowering strategy was proposed to improve the performance of NiFe-LDH based on a reverse relationship between lateral size and effective surface area. The increase in the latter parameter was speculated to greatly enhance hydroxyl ions in the feed. Another merit was the reduction in the catalyst layer film thickness, which lowered ohmic losses on the MEA. With this in mind, a one-spot spontaneous gelation-deflocculation method (Fig. 3a) was introduced to prepare ultra-fine NiFe-LDH particles with a small lateral size of less than 10 nm [103]. The as-prepared NiFe-LDH possessed both pronounced OER activity in half- and single cells over IrO_x, and required a low overpotential of 247 mV to reach 10 mA cm^{-2}, compared with 281 mV in IrO_x @ 10 mA cm^{-2}. In a full AEM cell, the MEA employing ultra-fine NiFe-LDH as the anode electrocatalyst (Fig. 3b) demonstrated superior performance, reaching 74.7% conversion efficiency and a cell voltage of 1.59 V under working conditions of 1.0 A cm^{-2} at 80 °C. This performance was acknowledged to be the highest among PGM-free catalyst decorated MEAs by far (Fig. 3c).

To further investigate the OER half-cell test and full AEM electrolyzer performance, various transition metal (Ni, Co and Fe) based oxides/hydroxides were prepared using a surfactant-free hydrothermal method [104–106]. Interestingly, the $NiFeO_xH_y$ oxyhydroxides exhibited the best OER performance in the half-cell, but the worst activity in the AEM stack. This may be due to the fact that $NiFeO_xH_y$ has poor electrical conductivity and no liquid electrolyte permeates to its surface. Therefore, only a portion of the total surface-active sites participated in the reaction. Using dry electrical conductivity as a reliable indicator, the effect of those oxides/hydroxides on the three-electrode system and AEM system performance can be better understood. Conductivity has a positive role by tuning the OER performance of those oxide/hydroxide materials. Intentionally anchoring Fe-species on the surface of the $NiCoO_x$ results in substantially improved activity on the $Fe/NiCoO_x$ because of the enhanced electrical conductivity. Thus, this finding may help establish the correlation between catalyst performance in the traditional three-electrode system and practical AEM system through the positive interaction on oxide/hydroxide catalyst interface. It also underlines the essential factor on the earth-abundant OER catalyst selection towards AEM utilization goal.

Although Ni/Fe-based materials have been widely investigated as OER catalysts, they are rarely studied for AEM electrolysis because of their poor stability. Further efforts should focus on composition, architecture and facile synthesis methods to enhance overall performance in practical devices.

3. Anion exchange membranes and ionomers

The anion exchange membrane (AEM) is one of the core components in AEM electrolysis systems. They transfer hydroxyl ions from the cathode chamber to the anode chamber, and prohibit gas crossover and electron transmission during practical electrochemical operation [107, 108]. AEMs are composed of a hydrocarbon polymer backbone as the main chain, and a side chain of anion exchange functional groups. The polymeric backbone typically uses polysulfone (PSF) or polystyrene (PS) to connect divinylbenzene (DVB), and typical ion exchange groups are those containing ammonium ($-NH_3^+$, $-RNH_2^+$, $-RN^+$, $=R_2N^+$) or phosphonium ($-R_3P^+$) groups [109,110]. Good ion exchange membranes should be qualified with the following properties, high permselectivity, good ionic conductivity, robust thermal and mechanical stability, and superior chemical stability [111–113].

Synthesizing viable anion exchange membranes for practical application remains challenging. It is particularly hard to balance the knotty issues of good mechanical stability and high ionic conductivity [114, 115]. While forming abundant ion exchange groups on the polymer backbone will increase ionic conductivity, it may also reduce the mechanical strength of the polymer main chain, by increasing excess water uptake [116,117]. The chemical stability of the AEM cannot always be guaranteed because of hydroxide attacks on the fixed ions [118]. Another crucial factor that hinders AEM development is the degradation of ammonium groups, which can proceed in two different ways, via Hofmann elimination and nucleophilic substitution [80,119].

With the current advances in computational quantum chemistry, first principles density functional theory (DFT) can be used to probe the correlations between ionic conductivity, chemical stability and the degradation mechanisms of the AEM. Some examples are explored in works [120–126], which are not discussed in detail here. However, most studies tend to utilize commercially available membranes to deal with electro-membrane processes, such as A-201 produced by Tokuyama Corporation, Japan [127]. Nonetheless, as novel membrane materials are proposed and evaluated, they hold promise for boosting the adoption of hydrogen energy.

To investigate the influence of applied period over the AEMs, several different AEM chemistries have been employed in AEM systems tests. PSF was selected as a polymer backbone and different cationic groups were grafted to the adjacent side chain on the benzyl position. The cationic groups, including quaternary benzyl trimethylammonium (TMA^+), quaternary benzyl quinuclidium ($ABCO^+$, a.k.a 1-azaoniumbicyclo[2.2.2]-octane), and quaternary benzyl 1-methylimidazolium ($1M^+$), are illustrated in Fig. 4 [128]. The chloromethylation and subsequent AEM formation based on the above reactants were characterized using ^1H NMR. The stability of the PSF AEMs was tested while maintaining a constant current density of 200 mA cm^{-2} for 6 h, and then the detected cell voltage was increased from 1.6 to 2.4 V. The postmortem analysis on the PSF AEMs suggested that CO_2 intrusion caused instability in the electrolyzer system during short term operation, while the irreversible performance loss could mainly be attributed to degradation of the polymer backbone. The close proximity of cationic groups along the polymer backbone could easily result in backbone degradation, because of ether and quaternary carbon hydrolysis [127]. Incorporating beta hydrogens spacers could mitigate the Hofmann elimination and improve cation stability. Other recent works [129–133] have reported that cation stability in AEMs can be remarkably enhanced with cation groups attached to the long alkyl pedant groups of the polymer backbone. This is a promising strategy for AEM water electrolyzers design.

N-spirocyclic quaternary ammonium (QA) salts have shown huge potential for improving alkaline stability as reported by Kreuer et al., 6-azonia-spiro[5.5]undecane (ASU) had the longest half-time of 110 h, which was superior to N,N-dimethylpiperidinium (DMP), N,N-d imethylpyrrolidinium (DMPy), 5-azonia-spiro[4.4]nonane (ASN), tetrapropylammonium (TPA), and N-benzyl-N-methylammonium (BMP) composite. This can be explained by the fact that the constrained ring conformation in the six-membered spirane ring system creates a huge transition state energy barrier for both the substitution and elimination reactions, as compared to the methyl groups [134].

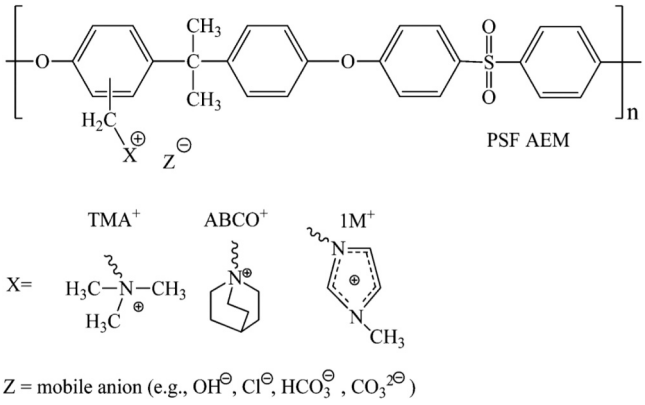

Fig. 4. Polysulfone based AEMs with quaternary benzyl ammonium and different imidazolium groups.
Reproduced with permission [128]. Copyright 2014, The Royal Society of Chemistry.

To introduce the N-spirocyclic QA cations into the polymers in a more straightforward way, a cyclo-polycondensation strategy was proposed to anchor the spiro-centered QA cations on the polymer chain, as schematically presented in Fig. 5. The "spiro-ionenes" type AEMs showed high thermal and alkaline stability in characterizations by NMR and SAXS. The AEMs exhibited no degradation for more than 1800 h in hydrogen isotope marked 1 M KOH electrolyte at 80 °C [135]. The viability of the spiro-ionenes in this work suggests a facile route to prepare highly OH^- conductive and alkali-stable AEMs materials.

González and Zhuang suggested that a benzyl-N-methylpyrrolidinium head-group should be considered to form pendent benzyl-QA types AEMs [136]. They proposed a radiation-grafting method to produce the benzyl-linked saturated-heterocyclic QA head groups. The two resulting AEMs of ETFE-g-poly(vinylbenzyl-N-methylpiperidinium)-QA and ETFE-g-poly (vinylbenzyl-N-methylpyrrolidinium)-QA had excellent alkaline stability, with a mere ca. 17–18% ion-exchange capacity loss, and that value was 30% higher than the benchmark benzyltrimethylammonium head-group functionalized AEMs. When benzyl-N-methypyrrolidinium head groups were employed in AEM fuel cells, they also yielded the high-performance efficiency of 980 and 800 mW cm^{-2} with PtRu/C, Pt/C acting as the anode and cathode, respectively, with PSF as the ionomer. Although the results in most works have agreed that the alkali instability originates with the positively charged N in the QA head groups at the benzyl position, extending the radiation-grafting method to prepare AEMs with non-benzyl-QA groups is still challenging. Yan et al. also reported a family of poly(aryl piperidinium) (PAP) AEMs/ionomers by grafting alkaline-stable piperidinium cations along the high-molecular-weight ether-bond-free, rigid and hydrophobic aryl backbone [19]. The inclusion of piperidinium cations into aryl polymer backbone improves the tradeoff between the hydroxide conductivity (> 50 mS cm^{-1}) and the dimensional stability, thus making high-molecular-weight PAP simultaneously demonstrates state-of-the-art chemical stability, hydroxide conductivity and mechanical robustness.

Ionomers generally act as bridges, serving as reliable conductors between AEMs and active sites on the surface of the catalyst layer [73, 78]. Ion exchange capacity (IEC) is a crucial parameter used to evaluate the performance of ionomers, and it can be tuned by grafting enormous ion exchange groups within the polymeric surface. The excess ion conductive groups can result in high water uptake in the ionomers, resulting in the further dissolution of the ionomers in the electrolyte, especially during operation at ascending temperatures [137]. The interface between the ionomers and polymer matrix is easily damaged. The interaction between them can improve the mechanical strength of the AEMs, while it also decreases chain mobility and the total pore volume of the AEMs [138]. Finding a suitable cross-linker to ensure high ionic conductivity and stability is extremely urgent as a result.

Recently, a series of trimethyl ammonium functionalized polystyrenes (in TMA-x, the x refers to the molar percentage of quaternized benzyl ammonium) were synthesized and used as ionomers (Fig. 6). The designed ionomeric binders were based on the following considerations. First, using aliphatic groups instead of phenyl groups in the polymer matrix can eliminate possible phenyl adsorption and the occurrence of acidic phenyl species. Next, employing TMA-x avoids the use of long non-ionic alkyl chains in the polymer backbone, which has been proven to substantially reduce polymer solubility in solvent. Third, ammonium or amine groups in the polymer side chain are beneficial to maintaining the high pH of the electrolyte.

The obtained hexamethyl trimethyl ammonium-functionalized Diels-Alder polyphenylene (HTMA-DAPP) AEMs reached a maximum IECs value at 3.3 mequiv. g^{-1}. Moreover, HTMA-DAPP had a notable hydroxide conductivity of 120 mS cm^{-1} at 80 °C. The polyphenylene backbone could be effectively manipulated to control and optimize the molecular weight of the HTMA-DAPP, which directly led to excellent mechanic strength (tensile stress >20 MPa at approximate 90%

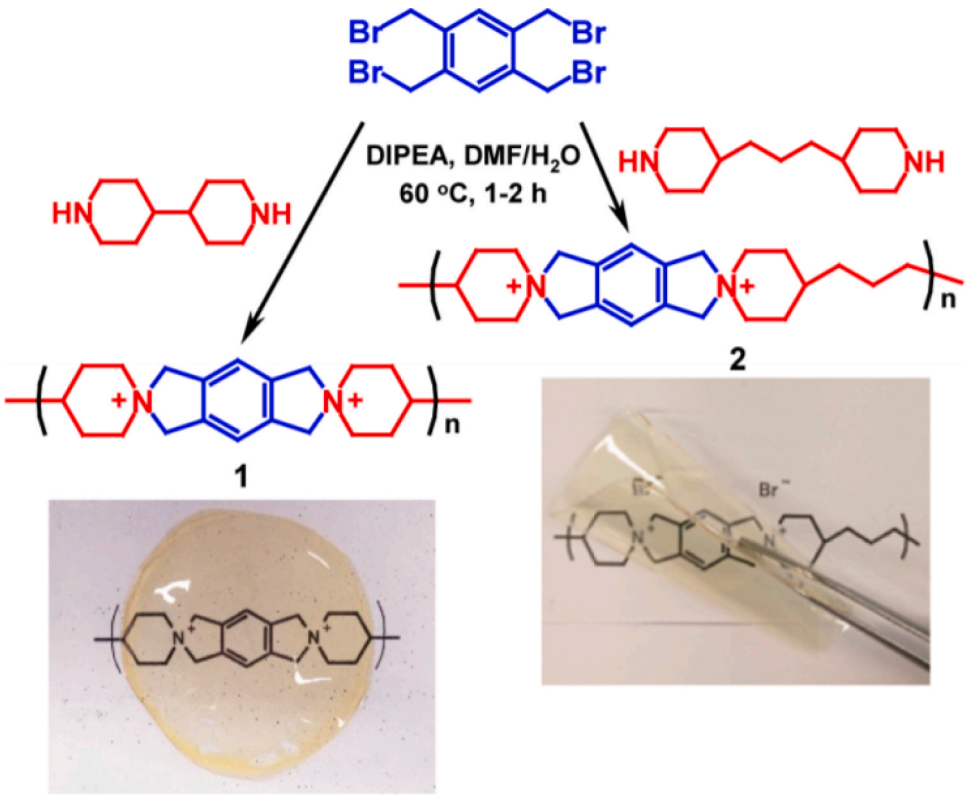

Fig. 5. Synthetic process of spiro-ionenes (1 and 2 type) via cyclopolycondensation of 4BMB with BP and TMDP, separately. Reproduced with permission [135]. Copyright 2017, American Chemical Society.

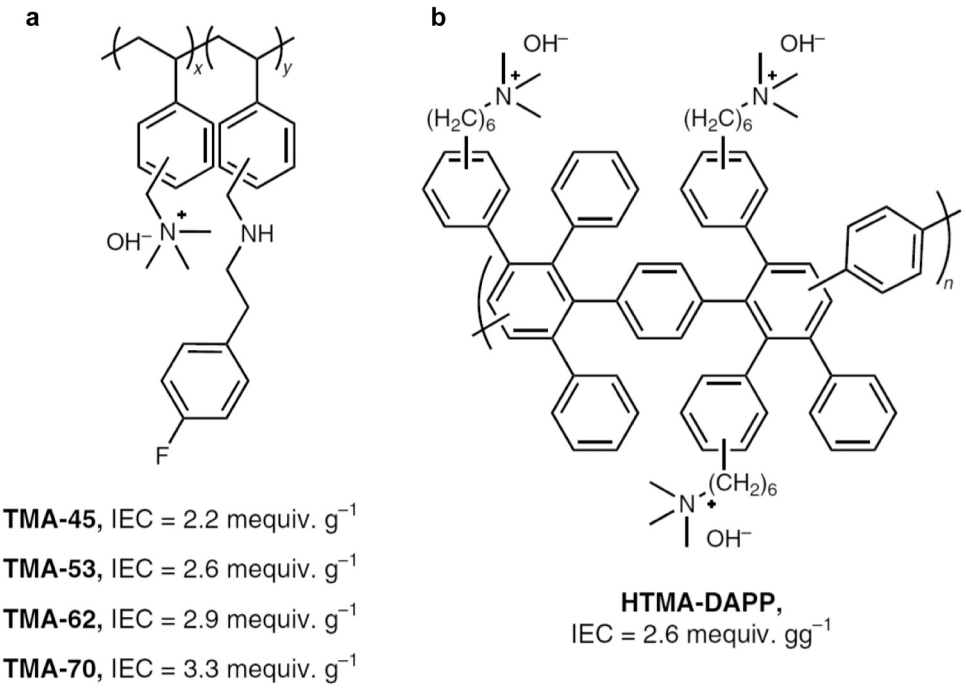

Fig. 6. The chemical structures: (a) trimethyl ammonium functionalized polystyrenes (TMA-x) ionomers; (b) hexamethyl trimethyl ammonium-functionalized Diels-Alder polyphenylene (HTMA-DAPP) AEMs.
Reproduced with permission [139]. Copyright 2020, Nature Publishing Group.

moisture at 50 °C) [139]. After assembling the HTMA-DAPP, Pt/Ru cathode and IrO_2 anode as the MEA, they were tested in a full AEM cell with pure water feed, and the MEA exhibited a current density of 107 mA cm^{-2} at 1.8 V and 60 °C. After determining the optimal ionomer content, the anode NiFe catalyst was further probed, and returned a high cell performance of 2.7 A cm^{-2} at 1.8 V in the newly constructed MEA during highest ionic concentration. This level of activity is even competetive with PEM electrolyzers, while using a PGM-free catalyst. However, for industrial application the instability of the constructed AEM electrolyzer system needs to be proved.

Tang et al. introduced a combined Menshutkin reaction and olefin metathesis to prepare anion conductive poly(2,6-dimethyl-phenylene oxide)s PPOs with bulky imidazolium cations as the ionomer [140]. The PPO-based AEMs had good mechanical properties (tensile stress> 20.8 MPa), and relatively low water uptake (ca 0.13.9 wt%). The PPOs' stable character was inherited from the imidazolium group, which exhibited no degradation in 1 M NaOH electrolyte at 80 °C. Moreover, The conductivity of the PPO-based AEMs was basically retained with no current density degradation after nearly 960 h operation. This may be correlated with the dedicated locations (C2, C4 and C5) of the imidazolium cations and the resulting crosslinked architecture. The special functionality enables the cationic center of the PPOs to avoid being attacked by H_2O and/or OH^-. The cell performance of PPO-based AEMs showed a peak power export of 173 mW cm^{-2} at 410 mA cm^{-2} and remained stable during operations at a constant 200 mA cm^{-2}. The lifespan of the crosslinked imidazolium was 3 times longer than that of the benzyltrimethylammonium functionalized PPO ionomer.

In practice, many factors can influence the performance of ionomers, not only cation cross-linkers but the polymer matrix itself [73]. Solvent type, catalyst coating method, operating temperature and catalyst character can all determine the extrinsic performance of ionomers [137, 141]. Prior to designing ionomers, researchers should think about the compatibility of all components in the AEM system as well as the expected performance levels.

4. Membrane electrode assembly and electrolyzer performance

An MEA is a collective system containing AEMs, ionomers, anode and cathode. The catalyst-coated substrate (CCS) and the catalyst-coated membrane (CCM) methods are commonly used to fabricate MEAs and assemble them into AEM cells for performance testing [142]. The CCM approach has received considerable attention, because it has unique advantages over CCS. During the CCM preparation process, the electrocatalyst and a binder were mixed to form a homogeneous ink, and then the ink was coated on both sides of the AEM by spraying. Mechanical or hot pressing was then used to treat the AEM after it was housed between the gas diffusion layers (GDLs). The widely adopted hot-press approach used in PEM cells was found not to be a good choice in AEM systems. The level of mechanical force and elevated temperature caused irreversible damage to the membrane, even though it was supported with metal-based electrode substrates (e.g., metal foams, Ti plates and stainless steel felt) [143–145]. In the CCS approach, the catalyst ink was directly deposited on the GDLs and then sintered, to obtain the gas diffusion electrodes (GDEs). The sandwiched GDLs, or GDEs with AEM as the inner layer, were then hot pressed to produce the ultimate MEA.

Various strategies have been explored to enhance the efficacy of AEM systems, and works related to MEA design will be discussed next.

In an attempt to develop novel MEA devices, Zhao et al. proposed the concept of the integrated inorganic membrane electrode assembly (I^2MEA) for AEM electrolysis systems [146]. Inorganic Mg-Al layered double hydroxides (Mg-Al LDHs) were used as the ionic conductor, and underwent a cold-pressed process to form a membrane. Subsequently, the PGM-free catalyst was coated on both sides of the membrane to form I^2MEA. The development of I^2MEA was guided by two objectives. The first was to avoid the complex yet toxic preparation process of conventional AEM cells, in which the chloromethylation, bromomethylation, quaternizataion, and alkalization steps were generally included. The second was to maintain robust stability and high hydroxide ion conductivity which the AEM system preferably requires.

During the I^2MEA based AEM setup, a series of operating conditions

and structural effects were probed. $CuCoO_x$ mixed oxides and Ni/(CeO_2-La_2O_3)/C were used as the anode and cathode catalysts at a loading of 40 mg_{cat} cm^{-2}, respectively. Nickel foam and carbon paper were chosen as GDLs for the anode and cathode counterparts. Titanium end plates with a circular single serpentine flow field were used to seal the I^2MEA and GDLs.

Many operating conditions have been reported to significantly affect AEM performance, including membrane thickness, electrolyte type, and operating temperature. Employing the novel I^2MEA fabrication approach, AEM cells were able to reach a peak current density of 208 mA cm^{-2} under 0.1 M NaOH electrolyte with a cutoff voltage of 2.2 V at 70 °C. Strikingly, the I^2MEA maintained pronounced stability after 600 h at a constant 80 mA cm^{-2} with decay parameters lower than 100 μV h^{-1}. The excellent stability was associated with the integrated architecture, which permitted the smooth diffusion of hydroxide ions. The I^2MEA design strategy is expected to shed light on other solid-state energy storage devices using solid electrolytes.

To obtain more details about the structure and morphology of catalyst layers prepared by the CCS method during practical AEM electrolysis, Bessarabov and coworkers introduced the SEM technique to study interface between the catalyst layers and the binder within the MEA [147]. Sustanion, AEMION and A-201 were used as membranes in the AEM electrolyzer, and Nafion was selected as the binder. $NiFe_2O_4$ on nickel and NiFeCo on stainless steel substrate were used as the anode and cathode, respectively. The impedance values of the Sustanion, AEMION and A-201 MEAs were 0.097, 0.120 and 0.133 Ω cm^2, respectively, in 1 M KOH electrolyte at 60 °C. This performance indicated the Sustanion membrane had higher ionic conductivity despite its being the thickest. The unique polymer resin morphology and boundary interaction during the interface could have been responsible for the small ionic resistance of the Sustanion membrane. However, the specific factor contributing to the difference in impedance remained unknown, due to the complex constitution of the MEAs. The AEM cell performance of the different MEAs were examined, and the Sustanion-based MEA exhibited the most pronounced electrocatalytic performance with an available current density of 300 mA cm^{-2} at 0.1 M KOH and 60 °C. The performances of AEMION and A-201 were inferior to the Sustanion-based MEAs.

Postmortem analysis of the Sustanion-based MEA under SEM indicated that the catalyst layers on the anode and cathode adhered robustly to the membrane surface, and retained their original morphology, with no cracks evident on the surface. In contrast, the AEMION- and A-201 membranes had irregular and dark areas showing the catalyst had peeled off from the membrane surface. This result indicated there was weak bonding interaction between the catalyst layers and the AEM membrane, which can happen in most MEAs, although the hot press method on CCS could improve cell performance and strengthen the membrane-catalyst surface. Bessarabov also reported that the delamination process of the AEMION-based and A-201-based MEAs may have been caused by incompatibility with the Nafion ionomers and the polymer resin, as previously reported in PEM fuel cells [148,149]. Another possible reason for the difference in MEA performance may be the difference in the thermal and hydrated expansion of the interface between the Nafion ionic binder and catalyst [150].

The CCM approach provides notable advantages, including intimate contact between the catalyst layer and polymer membrane, which normally results in higher MEAs ionic conductivity compared with those fabricated by CCS. The technical advantage of CCM allows the resulting MEA to maintain the overall performance of the AEM splitting system with lower catalyst loading [151].

However, the CCM method can also cause poor electrical contact between the MEA and current collector, an issue that will require the development of a suitable polymer binder for scalable application.

Spray coating and deposition are commonly used to transfer homogenous catalyst ink onto the surface of the AEMs [152–155]. Recently, Li et al. synthesized a series of piperidinium-functionalized poly(2,6-dimethyl phenylene oxide)s as AEMs, and then used CCM to coat the anode Pt catalyst and cathode AS-4 catalyst on the MEA surface. The formed MEA had hydroxide conductivity comparable to reported QA-based AEMs, of 29.0 mS cm^{-1} at 20 °C. To further check the cell performance of the CCM-MEA, a highly conductive LSCPi membrane based MEA was prepared, and achieved a current density of 300 mA cm^{-2} at 1.8 V at 50 °C with pure water as feed. The LSCPi membrane had robust stability, and retained 98% of its conductivity after a 560 h operation test in 1 M NaOH at 80 °C. Postmortem analysis suggested that the piperidinium cation functional groups on the LSCPi membrane determined the lifespan of the AEMs, as verified by NMR [143].

The electrodeposition of Ni species on carbon paper (CP) to prepare an MEA was also reported, with relatively low Ni loadings of 8.5 $μg_{Ni}$ cm^{-2} and uniform catalyst particle distribution. It was also claimed that the CCM-induced homogeneous catalyst distribution was beneficial, increasing the electrochemical surface area for gas evolution reactions [92]. The Ni/CP electrodes were used as both anode and cathode on the MEA, and the rationally fabricated MEA delivered a current density of 150 mA cm^{-2} at the applied cell voltage of 1.9 V at 50 °C. This result demonstrates that electrodeposition can be an effective and facile tool for precisely controlling the roughness and the catalyst loadings of the ultimate MEA. In spite of the Ni/CP based MEA's good cell performance, the stability test on the MEAs during operation was lacking.

The cell performance of MEAs fabricated with the CCS and CCM approaches were compared by Park [156]. In this research, the MEA fabrication method, operating conditions, and several parameters that influence AEM performance were probed. Electrochemical impedance spectroscopy (EIS) was utilized to distinguish the effect of the MEA fabrication approach on the resulting AEM performance. As indicated by the polarization curves in Fig. 8a, the AEM electrolyzer performance for the different MEA fabrication methods varied. The CCM based MEA had much higher performance (630 mA cm^{-2} at 1.9 V) than those fabricated with CCS (390 mA cm^{-2} at 1.9 V with hot pressing; less than 100 mA cm^{-2} at 1.9 V without hot pressing). In the CCS approach, the hot pressing treatment process was considered necessary to improve MEA performance.

The huge gap in performance between the CCM and CCS MEAs can be well explained by the Nyquist plots (Fig. 8b). The CCS without hot pressing process resulted in much higher ohmic resistance than CCM and CCS with hot pressing, and led to significantly lower electrolyzer performance. In contrast, MEAs based on the CCS approach with hot-pressing, and the CCM approach, basically exhibited the same ohmic resistances. This suggests that the hot pressing process was a prerequisite for good contact between the catalyst layers and the AEMs.

Moreover, when the CCS approach was combined with the hot pressing process it resulted in higher mass transport resistance, as revealed by the larger arc radius value in the low-frequency region. Likewise, the MEA obtained from the CCM method had the lowest ohmic resistance in the high-frequency region, charge transfer in the intermediate-frequency region, and mass transport resistances in the low-frequency region. Based on these results, the CCM method was acknowledged to be the optimal MEA fabrication approach for the AEM water electrolysis system.

Interestingly, Mamlouk et al. reported the opposite MEA performance trend for the CCS method and CCM method [157]. The polarization curves recorded for a $NiCo_2O_4$ catalyst applied by spraying directly on the GDL, and the CCM approach, were compared at different operating temperatures. To deliver a current density of 100 mA cm^{-2} at 60 °C in 0.1 M NaOH electrolyte, the GDL-spraying and CCM methods required voltages of 1.65 V and 1.69 V, respectively. These performance values were better than many on various non-noble catalysts reported in the literature, which generally required voltages ranging from 1.7 to 1.9 V to reach the same current density [158–160]. Meanwhile, the promising performance of the GDL-spray-based MEA in very low alkaline concentration suggests there is room for further improvement if the

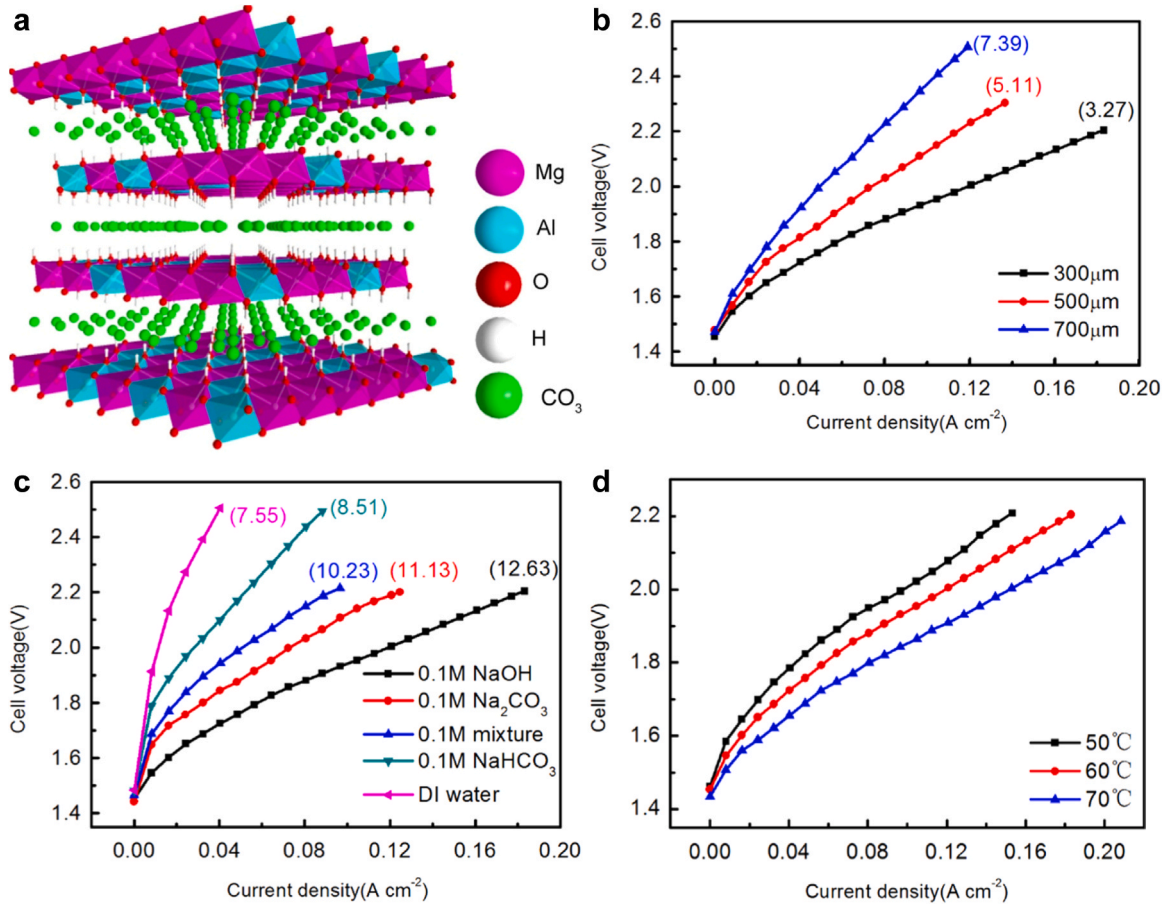

Fig. 7. (a) Crystalline structure of Inorganic Mg-Al layered double hydroxides (Mg-Al LDHs). Polarization curves of AEM electrolyzer based on I[2]MEAs under different operating conditions: (b) membrane thickness; (c) electrolyte feed; (d) operating temperature.
Reproduced with permission [146]. Copyright 2015, Elsevier Inc.

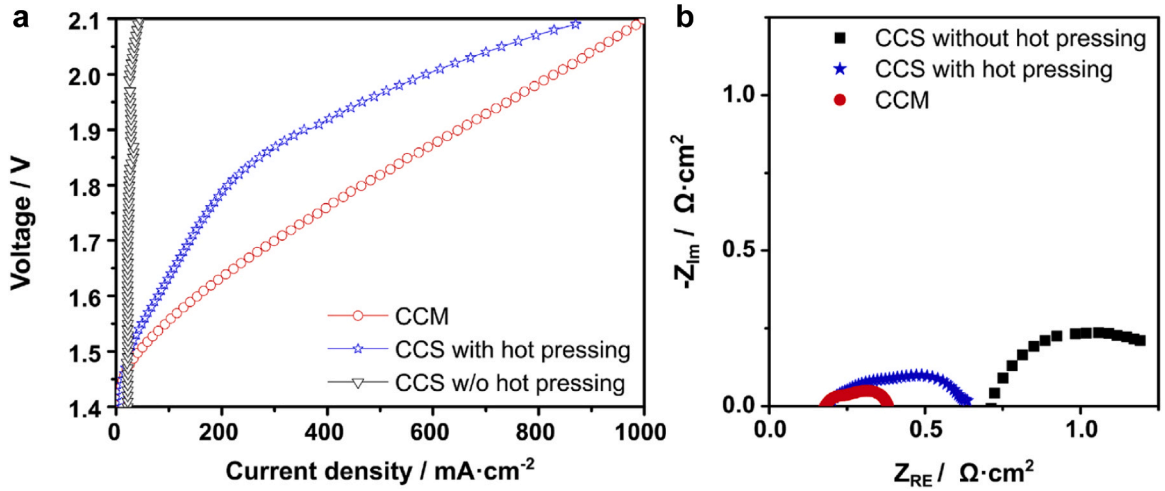

Fig. 8. (a) Polarization curves; (b) Nyquist plots of MEA fabricated with CCM and CCS with and without hot-pressing treatment.
Reproduced with permission [156]. Copyright 2019, Elsevier Inc.

$NiCo_2O_4$ particle size can be lowered to approximately10 nm.

5. Operating conditions

In addition to the abovementioned components which affect AEM electrolyzer performance, other operating conditions, including applied cell voltage, available current density, electrolyte temperature, chamber pressure, and electrolyte type, have a huge influence on AEM electrolysis activity. Those crucial parameters are discussed in the next section in detail.

5.1. Current density

In an integrated AEM water electrolysis cell, the applied cell voltage and available current density reflect the energy utilization efficiency and the ultimate hydrogen production yield of the electrolyzer system. A higher current density signifies faster water splitting efficiency. However, an ultra-higher current density may have an adverse effect on the cell, due to the extreme evolution of gas bubbles on the electrode surface, which in turn increases the overpotential required by the cell. Hence, most reported AEM electrolyzer maintain a regular current density of 100–500 mA cm^{-2}. When identifying the most suitable current density, consideration should include maximized hydrogen production yield and reasonable electric utilization efficiency.

5.2. Operating temperature

Operating temperature also positively affects AEM water electrolysis (AEMWEs) performance. The AEM electrolyzer normally operates within a temperature range of 50–80 °C. An increase in temperature can accelerate electron and mass transport during the electrochemical reaction, and in turn minimize the overpotential required by the MEAs. In the same work conducted by Park et al. [156], the temperatures of the electrolysis were set at 50, 60 and 70 °C to probe the available current density of the AEM at 1.9 V. Fig. 9a reveals the polarization curves of the AEMWEs operating at different temperatures. The cell performance improved with the increase in temperature. The current density obtained under 70 °C was 2.2 magnitude higher than the cell tested at 50 °C. Moreover, the ohmic resistance decreased markedly at elevated temperature (Fig. 9b), which also suggests the ionic conductivity on the MEA was enhanced at elevated temperature. This result is consistent with the experimental observations of other AEMs, such as I^2MEAs, R4-C12 and QPPO [146,161], in that the optimal operating temperature to induce superior performance was 70 °C.

In a work based on I^2MEAs, the cell efficiency of the AEMs was also linked to a positive relationship with increasing operating temperature. The increased temperature not only improved the ionic conductivity of the Mg-Al LDHs, but also ultimately led to a boost in the electrocatalytic behavior of the catalysts. The maximum current density of 208 mA cm^{-2} was reached at the applied conditions of 2.2 V at 70 °C (Fig. 7d). During operation at this current density value, large numbers of hydrogen gas bubbles evolved from the surface of the cathode. Despite this, the pronounced performance achieved here was still deemed promising given that the I^2MEAs consisted of non-PGM electrocatalysts and a thick inorganic membrane.

5.3. Operating pressure

Another predominant feature of AEM electrolysis is that the H_2 produced inside the cell/stack can be pressurized for favorable storage and utilization. The AEM system generally runs at pressures of 15–30 bars [93], and some specialized types can operate at more than 350 bars [162]. To function effectively at higher H_2 pressure, the cell components, the catalysts, sealing gasket, membrane, and current collectors, need to be specifically customized to the harsh operating condition. Recent studies have confirmed that operating pressurized AEM electrolysis at around 10 bars was possible without further component modification, due to the reliable mechanical robustness of the membrane and other components. Considering the evolution of H_2 inside the pressurized cathode chamber, there is a high possibility of H_2 cross-permeation through the AEM membrane which should be specially noticed and handled.

Ito et al. [163] systematically investigated the influence of H_2 pressure on electrolyzer performance by probing cell voltage, ohmic resistance, H_2 content in the anode gas, and so on. The H_2 pressures were set at 1.0, 5,0 and 8.5 bars in the cathode compartment, while atmospheric pressure was set on the anode. No remarkable difference in cell performance could be detected at the assigned H_2 pressures, while the maximum cell voltage difference at 1 A cm^{-2} was only 11 mV (Fig. 10).

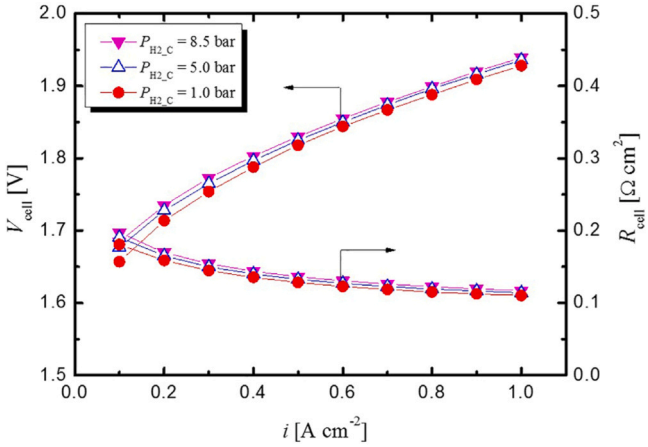

Fig. 10. Polarization curves and electrolyzer resistance characteristics under various operating pressures in the cathode chamber.
Reproduced with permission [156]. Copyright 2019, Elsevier Inc.

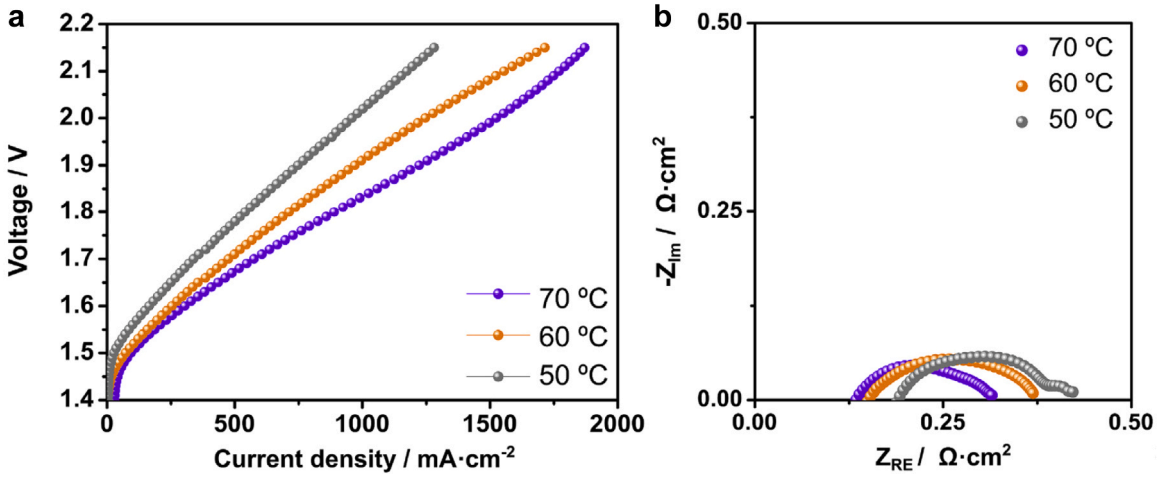

Fig. 9. (a) Polarization curves; (b) Nyquist plots of AEMWEs recorded at different cell operating temperatures (50, 60, and 70 °C).
Reproduced with permission [156]. Copyright 2019, Elsevier Inc.

This result clearly suggests that pressurized H_2 production may be realized without a significant increase in cell voltage. In addition, H_2 permeability across the anode chamber was found to be somewhat lower, only 0.16 times that of PEM systems. Also, the water content measured in the produced H_2 was low, proving that operating a pressurized AEM system could be an advantageous strategy for low humidity H_2 production, with minimum performance degradation.

5.4. Electrolyte

The electrolyte is an essential component in the AEM cell/stack and greatly determines the total performance of the electrolysis cell. The electrolyte conventionally used in the AEM system is composed of KOH at 30–40% concentration, 1 M KOH aqueous solution, ultrapure water, deionized water, 1 wt% K_2CO_3, and 1 wt% (K_2CO_3 + $KHCO_3$). Different electrolyte feeds in the AEM cell can affect the availability of hydroxyl ions on the MEA, and further influence AEM cell performance.

Ito and coworkers also probed how electrolyte type affected the performance of AEM [164,165]. Based on the experimental results, they reached the following conclusions. 1) AEM was difficult to operate with pure water due to the limited ions, and therefore hard to meet practical commercialization. 2) The K_2CO_3 solution can be selected as a reliable choice for excellent performance over the KOH solution only when the pH value of the electrolyte is restricted to mild alkaline values (pH ≤ 12). 3) The relative humidity of the H_2 gas (78–88%) produced from the cathode cell was easily affected by the electrolyte type and pressure conditions. To be specific, in a constructed AEM cell consisting of commercial A201 as the AEM, $CuCoO_x$ as the anode catalyst, Pt as the cathode catalyst, deionized water, dilute K_2CO_3 and KOH solutions were used as the electrolyte to prevent possible deterioration (pH > 14). The performance curve of the AEM was recorded under different cell potentials (V_{cell}) and cell resistances (R_{cell}) versus current density (i) during the practical AEM electrolysis. With the deionized water feed, the AEM reached a voltage of 2.2 V at the fairly low current density of 100 mA cm^{-2}.

Meanwhile, the detected R_{cell} value was very high (>1.4 Ω cm^2) but unstable. This means that the deionized water was not a suitable electrolyte candidate for high performance, as it is for PEM. On the other hand, the low concentration (0.1 wt%) K_2CO_3 solution led to remarkably superior performance compared with deionized water, and the obtained R_{cell} value was stable and lower (<0.5 Ω cm^2). The AEM cell also had improved performance when the K_2CO_3 concentration was increased from 1.0 wt% to 10 wt%. The cell reached a maximum of 1000 mA cm^{-2} at the cell voltage of 1.91 V.

The direct comparison of the K_2CO_3 (10 wt%) and KOH (10 mM) electrolytes is displayed in Fig. 11. Both solutions had approximately the same pH value (11.8 for K_2CO_3 and 12.0 for KOH). The KOH electrolyte resulted in inferior cell performance compared with the K_2CO_3 solution. This was attributed to the difference in R_{cell} and the internal pH condition with those two solutions. Further measurement with the KOH solution suggested that the AEM cell based on KOH required a longer response time to arrive at stable V_{cell} and R_{cell} values, compared with the cell driven by K_2CO_3. Accordingly, the K_2CO_3 solution was considered the most viable electrolyte for AEM electrolysis when the cell/stack was operated under mild alkaline conditions (pH ≤12). Faraj et al. [166] and Pavel et al. [93] also reported similar findings in previous examples, and concluded that the use of a mild alkaline electrolyte was more advantageous for system operation, as well as capital cost reduction, because it permitted the use of low-cost materials (stainless plate, pipes, and tanks).

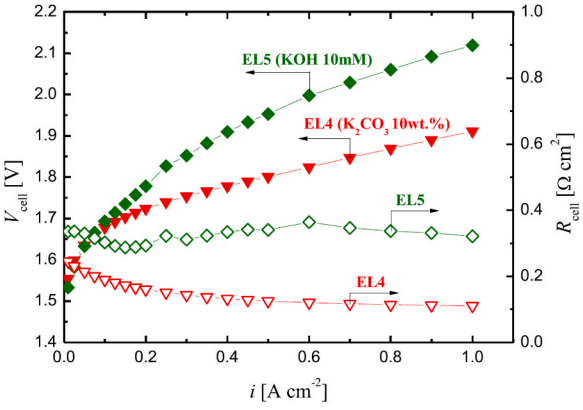

Fig. 11. The characteristic i-V_{cell} and i-R_{cell} curves operating under 10 wt% K_2CO_3 and 10 mM KOH electrolyte.
Reproduced with permission [165]. Copyright 2018, Elsevier Inc.

Fig. 7c also illustrates the functions of different electrolytes in an I^2MEAs based AEM system [146], where a 0.1 M NaOH, 0.1 M Na_2CO_3, 0.1 M mixture (Na_2CO_3 + $NaHCO_3$), 0.1 M $NaHCO_3$, and DI water were investigated. In their system, they found that the overpotential had a reverse trend with change in alkalinity, where a small pH value (<10) could induce a large overpotential. Also, the internal resistance of the electrolyte had a huge influence on performance improvement. The large OER potential was affected by a decrease in hydroxide ion concentration. Remarkably, the I^2MEAs system was able to operate with weak alkaline solutions, including pure water.

6. Cost evaluation of hydrogen production by AEM electrolyzers

Producing hydrogen with AEM electrolyzers using clean electricity instead of traditional hydrocarbon compounds represents a revolutionary step in energy uptake. To develop a reliable roadmap for hydrogen adoption, the U.S. Department of Energy (DOE) launched the Hydrogen Analysis (H2A) Project, which was intended to establish rigorous and consistent analyses of a wide range of hydrogen technologies [167–169]. Such modeling tools enable better validation of analytical studies used to assess the cost of hydrogen production and delivery. To estimate the cost of hydroproduction from different approaches, a benchmark was estabilished based on the total cost of producing hydrogen by the steam methane reforming (SMR) process at 1.38 $ kg^{-1}. The cost is higher, 1.97 $ kg^{-1}, if the price of carbon is counted, at 50 $ t^{-1} CO_2. To sketch the contours of a competitive version of AEM electrolyzers, the performance of the electrocatalyst, the stack cost, and system durability are included.

6.1. Cost tradeoff based on performance and durability

Based on the modeled H2A hydrogen production scenario, Yan et al. [170] proposed an assumption to evaluate the cost tradeoff between performance and durability in low-temperature electrolyzers (i.e., a PEM electrolyzer, alkaline electrolyzer and AEM electrolyzer). The entire evaluation system was realized by assuming 20 $ MW h^{-1} electricity use with 40% capacity factor, to meet the massive hydrogen production goal set by the U.S. DOE and the corresponding H2A analysis system [169]. For the PEM and AEM electrolyzer, the stack cost was converted into an active area factored basis ($ m^{-2}), and the operating conditions, especially the current, were optimized to minimize hydrogen cost.

Meanwhile, the performances of the PEM and AEM electrolyzers were studied by considering the fixed direct current (DC) resistance value of 0.2 Ω cm^{-2} and different open-circuit voltages (OCV). With this model, the cost and performance of the membrane based electrolyzer followed a linear polarization relationship with the two aforementioned parameters, in a 10 year durability hypothesis (Fig. 12a). The proposed estimation model is also adaptable to any DC resistance value by scaling up the total cost in an inverse way.

The PEM electrolyzer stack cost in the H2A scenario was approximated to be around 4000 $ m^{-2}, which is more expensive than the

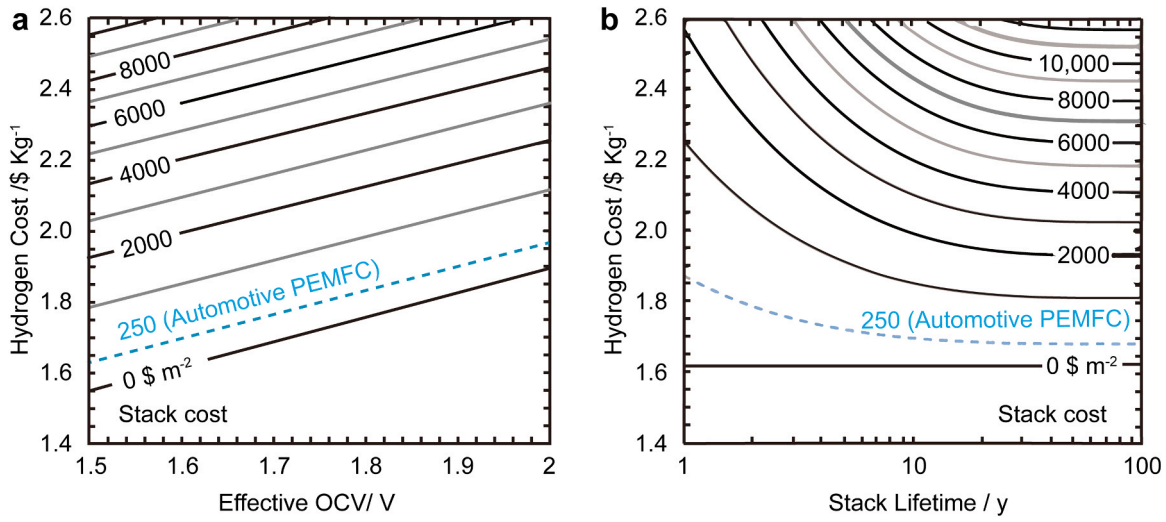

Fig. 12. Hydrogen production cost estimation at performance and durability tradeoff for low-temperature electrolyzer: (a) Cost analysis based on electrolyzer performance at a fixed 10 year stack durability; (b) Cost evaluation considering stack life factor at 1.6 V effective OCV.
Reproduced with permission [170]. Copyright 2019, Wiley-VCH.

manufacturing cost (250 $ m^{-2}) of proton exchange membrane fuel cells (PEMFCs) with their higher operating pressure, additional titanium plate usage, large electrocatalyst loading amount, and thicker proton exchange membrane. Accordingly, the AEM electrolyzer with reduced materials cost was still approximately 4–8 times higher in cost than the PEMFCs. The proper H_2 production cost would be located in the range of \$1.81-\$2.00 kg^{-1}. The capital cost and DC resistance are also important when estimating the ultimate hydrogen production cost, as shown in Fig. 12a. A 5% hydrogen cost is associated with the stack system, as predicted by the H2A scenario [169]. This difference can be explained by the following facts. First, insufficient capacity results in a higher capital cost contribution. Next, the reduced electricity price cuts down the electricity portion. More importantly, a cost tradeoff between electricity consumption and capital cost can be achieved by setting a different operating voltage. For perspective, the additional electricity and stack cost doubled the cost of practical hydrogen production.

The effect of stack cost and durability on the resulting hydrogen production can be seen in Fig. 12b, assuming a 1.6 V effective OCV. Durability is suggested to be crucial parameter with respect to hydrogen cost. In greater detail, taking the 2000 $ m^{-2} stack line and 10 year durablity as an example, a 1% price increase in stack cost could cut durability down by 2.7%. Here, the AEM electrolyzer may enable a favorable cost-durability tradeoff because it offers the possibility of using less costly stack materials. However, the cost reduction effort should be considered in a whole, and the durability issue require to be satisfied among other considerations.

6.2. *Cost tradeoff based on performance and electrocatalyst*

In a further effort, Yan et al. [170] also systematically studied the effect of electrocatalyst on the resulting hydrogen production cost, by considering the electrocatalyst's cost and corresponding performance. Here, the catalyst cost is determined on an electrode volume basis ($ cm^{-3}), and catalyst performance is expressed by comparing the overpotential to arrive at the fixed volumeric current density of 500 A cm^{-3}, which can generally be calculated from the Tafel plot. The overpotential

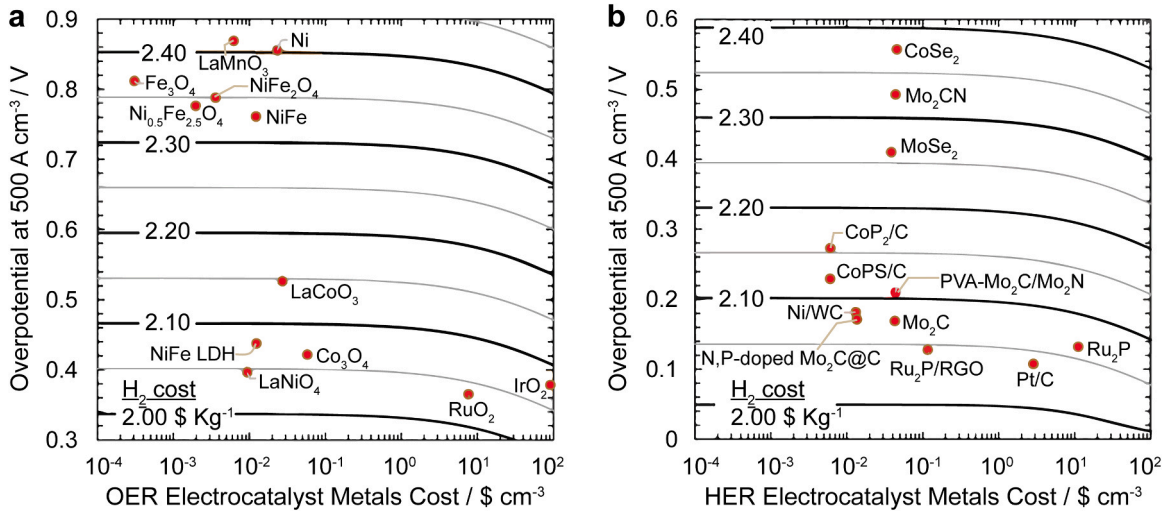

Fig. 13. Contour graph of electrocatalyst cost-performance tradeoff for AEM electrolyzer: (a) Hydrogen production cost versus OER electrocatalysts cost and performance with 20% Pt/C as cathode benchmark electrocatalyst; (b) Impact of HER electrocatalysts cost and performance by assuming RuO_2 as anode benchmark electrocatalyst.
Reproduced with permission [170]. Copyright 2019, Wiley-VCH.

values of OER and HER electrocatalysts were probed using Pt/C and RuO_2 as the cathode and anode electrocatalysts, respectively (Fig. 13) [171,172].

Twelve different electrocatalysts were selected for both OER and HER reactions (Fig. 13) to estimate hydrogen production cost. The electrodes were assumed to consist of 20% electrocatalysts, and costs are determined using the commerical metal price without including processing cost [173,174]. Pt/C and RuO_2 are typically regarded the best HER and OER electrocatalysts because they can maintain high activity under practical conditions. For most PGM-free electrocatalysts, a decrease in activity reduces cost saving, and thus leads to higher hydrogen production cost. As the OER electrocatalysts, NiFe LDH [175], Co_3O_4 [172] and $LaNiO_3$ [176] have a narrow hydrogen cost difference of 0.02 \$ kg^{-1} (Fig. 13a). The variation in cost is due to different performance. An overpotential of 100 mV resulted in an 0.08 \$ kg^{-1} change in hydrogen cost, which is equal to a 5–10 year difference in stack system durability. Therefore, considering that electrocatalysts may exhibit an order of magnitude difference in durability, for practical hydrogen production, the first priority should be durability, followed by performance, with the cost issue last.

All of the electrocatalyst pairs showed a hydrogen production cost higher than 2 \$ kg^{-1} as displayed in Fig. 13. In the previous discussion, Ni-based electrocatalysts exhibited more stable performance than RuO_2 in an alkaline environment, while their durability for up to several years requires further investigation. It is expected that the durability parameter will become the crucial factor in the development of PGM-free electrocatalysts. Assuming AEM the electrolyzer employees RuO_2 as the anode electrocatalyst, and an Ni-based sample (NiFe [175] or Ni/WC@C composite [177]) as the cathode material, the hydrogen production cost can be approximated to be 2.38 \$ kg^{-1}. This is a reasonable cost prediction for producing hydrogen in an industrial AEM electrolyzer. Further improvement in the durability of the PGM-free electrocatalysts is urgently needed to make the SMR hydrogen production process cost competitive.

7. Current analysis of research status of AEM systems

The current state of AEM electrolyzer research is presented in sporadic literature reports, mainly focusing on electrocatalyst developments and membrane designs. This can be observed using the Web of Science website: inserting the key words“anion exchange membrane water electrolysis” in the title blank only yields 35 papers over a 10 year period from 2010 to 2020, even though recent research in AEM electrolysis has been significantly boosted by the U.S. DOE efforts [167] and the FCH-JU funding project of the European Union (EU) [173].

In contrast, literature search involving separate HER/OER catalysts, ionomers, membranes and MEAs totaled more than 40,000+ titles. The plausible analysis to explain the research gap between core components and integrated AEM stacks can be attributed to the system complexity, and the lack of standard evaluation criteria. For example, most HER and OER electrocatalysts are reported to have excellent activity when they are tested at room temperature, for short duration time at low working voltage. However, in practical operation, to work efficiently both the anode and cathode electrocatalysts require conditions of 50–70 °C under a higher operating voltage (>1.8 V) and must perform for 10 years or longer [178].

Nevertheless, assuming that OER and HER electrocatalysts are able to withstand the abovementioned test conditions and show superior performance. Once they are assembled with the AEM membrane to form the MEA, membrane stability and ionic conductivity become further knotty issues for needing further development. The gas crossover issue and hydrogen storage also need special attention.

More importantly, no plausible performance criteria have been estabilished to date to standardize performance evaluation, cost estimation, gas purity, operating mechanism and so on. In brief, developing a promising AEM electrolyzer requires researchers have an integral understanding of the characteristics and mechanism of all of the components in AEM system. Hence, an assembled contribution from our research community is imperative to establish a systematic research roadmap for scalable hydrogen production using AEM electrolysis technology.

8. Summary

Although many advances have been made in the development of all the components in the AEM system, and have collectively improved cell/stack performance, the AEM electrolysis technology is still undergoing an initial stage of development. In this review paper, we have thoroughly discussed the main components of AEM electrolyzers, including HER/OER catalysts, AEM membrane, ionomer, MEA and electrolyzer performance. We have highlighted areas of progress and the utilization of low-cost materials, especially, PGM-free electrocatalysts, and reviewed the collective contributions of AEMs and ionomers on AEM activity. The CCS and CCM MEA fabrication methods were also presented. The influence of other critical parameters, including current density, operating temperature, H_2 pressure and electrolyte type, were also subsequently reviewed. The remaining challenges and special foci of current AEM electrolysis techniques are as follows.

8.1. OER and HER catalysts

The OER catalysts used in AEM systems are mainly based on Ni species and rare earth metals. OER kinetics can be easily affected by excessive catalyst loading at the anode, and lower utilization rate, especially when the concentration of hydroxyl ions in the electrolyte has decreased, and active sites on the catalyst have been blocked by the unavoidable high pressure of gas evolved in the MEA. Ni-Mo alloyed materials [94], Co_3O_4 nanocrystals [179], Fe and Ni-Fe alloys have been found to exhibit pronounced OER performance, however, longer stability up to thousand hours needs to be probed.

HER catalyst development should also focus simultaneously on low cost character and enhanced catalytic activity. Besides that, their stability and utilization efficiency are also required and ensured for practical utilization.

8.2. AEM membrane and ionomer

The development of advanced AEM membranes and ionomers with enhanced ion conductivity, hydroxyl ion selectivity as well as robust stability at higher operating temperatures (>60 °C) is critical to practical adoption. To minimize AEM degradation caused by nucleophilic attack and Hoffmann elimination of fixed cationic groups on the polymeric backbone, novel AEMs could adopt a imidazolium-functionalized or sulfonated poly(ether ether ketone) backbone. Side chains containing polar electron-donating groups and styrenic diblock copolymer with quaternary ammonium-functionalized hydrophilic block and hydrophobic block are also worth considering.

In addition, a systematic characterization method to study the properties of AEMs based on polarization curves, EIS, in-situ/ex-situ electronic microscopy, chronoamperometry, and gas crossover analysis should be developed, for clearer understanding of AEMs interactions with the aforementioned degradation factors.

8.3. Characterization and cell performance of the MEA

The physical characterization and electrochemical investigations of MEAs have demonstrated that both the CCM and CCS fabrication approaches can enhance overall AEM performance, but CCM is the preferable method because it helps maintain superior ionic conductivity. This phenomenon is suggested to be more advantageous than the interior improved electronic conductivity.

Nonetheless, the degradation mechanisms and interactions between

the AEM membrane and ionomers are poorly understood. More advanced characterization techniques and electrochemical probing methods, including operando FT-IR spectroscopy, in-situ TEM visualization, and EIS analysis, are urgently required.

Up to now, the best well-acknowledged cell performance of an AEM is 2.7 A cm^{-2} at 1.8 V, based on the HTMA-DAPP membrane, with NiFe and PtRu as the anode and cathode catalysts, pure water as the electrolyte at temperature of 85 °C. Most performance values reported in the laboratory have been inferior to AEM cells assembled with the commercial materials. This calls for more revolutionary effort to be paid not only to materials development and AEM characterization techniques, but also the combined use of empirical and theoretic approaches to predict optimum operating parameters.

9. Conclusions and perspectives

Hydrogen produced by PEM and AEM electrolysis is expected to become a larger share of the global hydrogen market, because they offer notable environmental advantages over the conventional hydrocarbon extraction method. An AEM electrolyzer can be integrated with intermittent energy resources and this would greatly lower the total cost of the cell/stack. Moreover, the system also offers great flexibility, including the ability to use compressed hydrogen storage cylinders for facile hydrogen utilization, or not. The produced high-purity hydrogen can be directly used in many fields, such as fuel cells and chemical hydrogenation.

However, at this stage in development, research and development should include a integration of technology development on these critical components to achieve significant deployment and market penetration at megawatt scale. Especially, improving durability and lifetime of AEM is critically important to fit industrial operating conditions. The swelling issue of AEMs in alkaline electrolyte should be resolved to improve stability against reactive oxygen species. Also, a standard accelerated stress test need to be proposed from both academic research society and industry. It is crucial for the determination of targeted lifetime (>10,000 h) on AEMs. Finally, it should be noted that laboratory developed AEMs have recently shown competetive performance over some commercial ones, implying that there is a huge room for the further advancement of AEMs.

Declaration of Competing Interest

The authors declare that they have no known competing financial interests or personal relationships that could have appeared to influence the work reported in this paper.

Acknowledgments

This research was supported by the Creative Research Initiative (CRI, 2014R1A3A2069102), BK21 PLUS (5120200413798) and Science Research Center (SRC, 2016R1A5A1009405) programs through the National Research Foundation (NRF) of Korea.

References

[1] M.G. Schultz, T. Diehl, G.P. Brasseur, W. Zittel, Air pollution and climate-forcing impacts of a global hydrogen economy, Science 302 (2003) 624–627.
[2] F. Sun, C. Li, B. Li, Y. Lin, Amorphous MoS_x developed on $Co(OH)_2$ nanosheets generating efficient oxygen evolution catalysts, J. Mater. Chem. A 5 (2017) 23103–23114.
[3] G.-F. Han, F. Li, W. Zou, J.-P. Jeon, S.-W. Kim, S.-J. Kim, Y. Bu, Z. Fu, Y. Lu, S. Siahrostami, J.-B. Baek, Building and identifying highly active oxygenated groups in carbon materials for oxygen reduction to H_2O_2, Nat. Commun. 11 (2020) 2209.
[4] B.M. Hunter, H.B. Gray, A.M. Muller, Earth-abundant heterogeneous water oxidation catalysts, Chem. Rev. 116 (2016) 14120–14136.
[5] L. Dai, Y. Xue, L. Qu, H.-J. Choi, J.-B. Baek, Metal-free catalysts for oxygen reduction reaction, Chem. Rev. 115 (2015) 4823–4892.
[6] P. Thangavel, M. Ha, S. Kumaraguru, A. Meena, A.N. Singh, A.M. Harzandi, K. S. Kim, Graphene-nanoplatelets-supported NiFe-MOF: high-efficiency and ultra-stable oxygen electrodes for sustained alkaline anion exchange membrane water electrolysis, Energy Environ. Sci. 13 (2020) 3447–3458.
[7] L. Wang, T. Weissbach, R. Reissner, A. Ansar, A.S. Gago, S. Holdcroft, K. A. Friedrich, High performance anion exchange membrane electrolysis using plasma-sprayed, non-precious-metal electrodes, ACS Appl. Energy Mater. 2 (2019) 7903–7912.
[8] S. Noh, J.Y. Jeon, S. Adhikari, Y.S. Kim, C. Bae, Molecular engineering of hydroxide conducting polymers for anion exchange membranes in electrochemical energy conversion technology, Acc. Chem. Res. 52 (2019) 2745–2755.
[9] J.A. Turner, Sustainable hydrogen production, Science 305 (2004) 972–974.
[10] B.C.H. Steele, A. Heinzel, Materials for fuel-cell technologies, Nature 414 (2001), 345-52.
[11] Y. Zhou, C.-H. Wang, W. Lu, L. Dai, Recent advances in fiber-shaped supercapacitors and lithium-ion batteries, Adv. Mater. 32 (2020), 1902779.
[12] I.V. Pushkareva, A.S. Pushkarev, S.A. Grigoriev, P. Modisha, D.G. Bessarabov, Comparative study of anion exchange membranes for low-cost water electrolysis, Int. J. Hydrog. Energy 45 (2020) 26070–26079.
[13] C. Li, Y. Liu, L. Guan, K. Li, G. Wang, Y. Lin, Understanding coordination modification strategy on metal organic framework-based system for efficient water oxidation, Chem. Eng. J. 400 (2020), 125884.
[14] C. Li, C. He, F. Sun, M. Wang, J. Wang, Y. Lin, Incorporation of Fe_3C and pyridinic N active sites with a moderate N/C ratio in Fe-N mesoporous carbon materials for enhanced oxygen reduction reaction activity, ACS Appl. Nano Mater. 1 (2018) 1801–1810.
[15] J.E. Park, M.-J. Kim, M.S. Lim, S.Y. Kang, J.K. Kim, S.-H. Oh, M. Her, Y.-H. Cho, Y.-E. Sung, Graphitic carbon nitride-carbon nanofiber as oxygen catalyst in anion-exchange membrane water electrolyzer and rechargeable metal-air cells, Appl. Catal. B Environ. 237 (2018) 140–148.
[16] C. Li, X. Zhao, Y. Liu, W. Wei, Y. Lin, 3D Ni-Co sulfoxide nanosheet arrays electrodeposited on Ni foam: a bifunctional electrocatalyst towards efficient and stable water splitting, Electrochim. Acta 292 (2018) 347–356.
[17] F. Li, G.-F. Han, H.-J. Noh, I. Ahmad, I.-Y. Jeon, J.-B. Baek, Mechanochemically assisted synthesis of a Ru catalyst for hydrogen evolution with performance superior to Pt in both acidic and alkaline media, Adv. Mater. 30 (2018), 1803676.
[18] G.M. Carlos, S. Lucas-Alexandre, X. Hu, Nanostructured hydrotreating catalysts for electrochemical hydrogen evolution, Chem. Soc. Rev. 43 (2014) 6555–6569.
[19] J. Wang, Y. Zhao, B.P. Setzler, S. Rojas-Carbonell, C.B. Yehuda, A. Amel, M. Page, L. Wang, K. Hu, L. Shi, S. Gottesfeld, B. Xu, Y. Yan, Poly (aryl piperidinium) membranes and ionomers for hydroxide exchange membrane fuel cells, Nat. Energy 4 (2019) 392–398.
[20] Y.S. Park, M.J. Jang, J. Jeong, S.M. Park, X. Wang, M.H. Seo, S.M. Choi, J. Yang, Hierarchical chestnut-burr like structure of copper cobalt oxide electrocatalyst directly grown on Ni foam for anion exchange membrane water electrolysis, ACS Sustain. Chem. Eng. 8 (2020) 2344–2349.
[21] Y.S. Park, J. Lee, M.J. Jang, J. Yang, J. Jeong, J. Park, Y. Kim, M.H. Seo, Z. Chen, S.M. Choi, High-performance anion exchange membrane alkaline seawater electrolysis, J. Mater. Chem. A 9 (2021) 9586–9592.
[22] I. Vincent, A. Kruger, D. Bessarabov, Development of efficient membrane electrode assembly for low cost hydrogen production by anion exchange membrane electrolysis, Int. J. Hydrog. Energy 42 (2017) 10752–10761.
[23] N.S. Lewis, Toward cost-effective solar energy use, Science 315 (2007) 798–801.
[24] M. Carmo, D.L. Fritz, J. Mergel, D. Stolten, A comprehensive review on PEM water electrolysis, Int. J. Hydrog. Energy 38 (2013) 4901–4934.
[25] E. López-Fernández, J. Gil-Rostra, C. Escudero, I.J. Villar-García, F. Yubero, A. de Lucas Consuegra, A.R. González-Elipe, Active sites and optimization of mixed copper-cobalt oxide anodes for anion exchange membrane water electrolysis, J. Power Sources 485 (2021), 229217.
[26] E. López-Fernández, J. Gil-Rostra, J.P. Espinós, A.R. González-Elipe, F. Yubero, A. de Lucas-Consuegra, $CuxCo_{3-x}O_4$ ultra-thin film as efficient anodic catalysts for anion exchange membrane water electrolysers, J. Power Sources 415 (2019) 136–144.
[27] M. Mandal, Recent advancement on anion exchange membranes for fuel cell and water electrolysis, ChemElectroChem 8 (2021) 36–45.
[28] I. Vincent, D. Bessarabov, Low cost hydrogen production by anion exchange membrane electrolysis: a review, Renew. Sustain. Energy Rev. 81 (2018) 1690–1704.
[29] C. Li, F. Sun, Y. Lin, Refining cocoon to prepare (N, S, and Fe) ternary-doped porous carbon aerogel as efficient catalyst for the oxygen reduction reaction in alkaline medium, J. Power Sources 384 (2018) 48–57.
[30] J. Lee, H. Jung, Y.S. Park, S. Woo, N. Kwon, Y. Xing, S.H. Oh, S.M. Choi, J. W. Han, B. Lim, Corrosion-engineered bimetallic oxide electrode as anode for high-efficiency anion exchange membrane water electrolyzer, Chem. Eng. J. (2020), 127670.
[31] B. Dou, H. Zhang, Y. Song, L. Zhao, B. Jiang, M. He, C. Ruan, H. Chen, Y. Xu, Hydrogen production from the thermochemical conversion of biomass: issues and challenges, Sustain. Energy Fuels 3 (2019) 314–342.
[32] B. Dou, H. Zhang, G. Cui, Z. Wang, B. Jiang, K. Wang, H. Chen, Y. Xu, Hydrogen production by sorption-enhanced chemical looping steam reforming of ethanol in an alternating fixed-bed reactor: Sorbent to catalyst ratio dependencies, Energy Convers. Manag. 155 (2018) 243–252.
[33] D. Pan, Z. Han, Y. Miao, D. Zhang, G. Li, Thermally stable TiO_2 quantum dots embedded in SiO_2 foams: characterization and photocatalytic H_2 evolution activity, Appl. Catal. B Environ. 229 (2018) 130–138.

[34] J. Yuan, C. Wang, Y. Liu, P. Wu, W. Zhou, Tunable photocatalytic HER activity of single-layered TiO_2 nanosheets with transition-metal doping and biaxial strain, J. Phys. Chem. C 123 (2019) 526–533.

[35] L. Ji, Y. Zhang, S. Miao, M. Gong, X. Liu, In situ synthesis of carbon doped TiO_2 nanotubes with an enhanced photocatalytic performance under UV and visible light, Carbon 125 (2017) 544–550.

[36] W. Fan, Q. Lai, Q. Zhang, Y. Wang, Nanocomposites of TiO_2 and reduced graphene oxide as efficient photocatalysts for hydrogen evolution, J. Phys. Chem. C 115 (2011) 10694–10701.

[37] H. Razavi-Khosroshahi, K. Edalati, M. Hirayama, H. Emami, M. Arita, M. Yamauchi, H. Hagiwara, S. Ida, T. Ishihara, E. Akiba, Z. Horita, M. Fuji, Visible-light-driven photocatalytic hydrogen generation on nanosized TiO_2-II stabilized by high-pressure torsion, ACS Catal. 6 (2016) 5103–5107.

[38] C. Yang, J. Qin, Z. Xue, M. Ma, X. Zhang, R. Liu, Rational design of carbon-doped TiO_2 modified g-C_3N_4 via in-situ heat treatment for drastically improved photocatalytic hydrogen with excellent photostability, Nano Energy 41 (2017) 1–9.

[39] Q. Tay, P. Kanhere, C.F. Ng, S. Chen, S. Chakraborty, A.C.H. Huan, T.C. Sum, R. Ahuja, Z. Chen, Defect engineered g-C_3N_4 for efficient visible light photocatalytic hydrogen production, Chem. Mater. 27 (2015) 4930–4933.

[40] C. Prasad, H. Tang, Q. Liu, I. Bahadur, S. Karlapudi, Y. Jiang, A latest overview on photocatalytic application of g-C_3N_4 based nanostructured materials for hydrogen production, Int. J. Hydrog. Energy 45 (2020) 337–379.

[41] H.A. Miller, K. Bouzek, J. Hnat, S. Loos, C.I. Bernäcker, T. Weißgärber, L. Röntzsch, J. Meier-Haack, Green hydrogen from anion exchange membrane water electrolysis: a review of recent developments in critical materials and operating conditions, Sustain. Energy Fuels 4 (2020) 2114–2133.

[42] N. Ramaswamy, S. Mukerjee, Alkaline anion-exchange membrane fuel cells: challenges in electrocatalysis and interfacial charge transfer, Chem. Rev. 119 (2019) 11945–11979.

[43] L. An, T.S. Zhao, Z.H. Chai, P. Tan, L. Zeng, Mathematical modeling of an anion-exchange membrane water electrolyzer for hydrogen production, Int. J. Hydrog. Energy 39 (2014) 19869–19876.

[44] P. Chen, X. Hu, High-efficiency anion exchange membrane water electrolysis employing non-noble metal catalysts, Adv. Energy Mater. 10 (2020), 2002285.

[45] J.H. Russell, L.J. Nuttall, A.P. Fickett, Hydrogen generation by solid polymer electrolyte water electrolysis, Am. Chem. Soc. Div. Fuel Chem. Prepr. 18 (1973) 24–40.

[46] W.T. Grubb, Ionic migration in ion-exchange membranes, J. Phys. Chem. 63 (1959) 55–67.

[47] W.T. Grubb, Batteries with solid ion exchange electrolytes I. secondary cells employing metal electrodes, J. Electrochem. Soc. 106 (1959) 275–278.

[48] S. Sun, Z. Shao, H. Yu, G. Li, B. Yi, Investigations on degradation of the long-term proton exchange membrane water electrolysis stack, J. Power Sources 267 (2014) 515–520.

[49] K. Ayers, N. Danilovic, R. Ouimet, M. Carmo, B. Pivovar, M. Bornstein, Perspectives on low-temperature electrolysis and potential for renewable hydrogen at scale, Annu Rev. Chem. Biomol. Eng. 10 (2019) 219–239.

[50] S. Siracusano, V. Baglio, N. Briguglio, G. Brunaccini, A. Di Blasi, A. Stassi, R. Ornelas, E. Trifoni, V. Antonucci, A.S. Aricòa, An electrochemical study of a PEM stack for water electrolysis, Int. J. Hydrog. Energy 37 (2012) 1939–1946.

[51] Ö.F. Selamet, F. Becerikli, M.D. Mat, Y. Kaplan, Development and testing of a highly efficient proton exchange membrane (PEM) electrolyzer stack, Int. J. Hydrog. Energy 36 (2011) 11480–11487.

[52] A. Ursua, L.M. Gandia, P. Sanchis, Hydrogen production from water electrolysis: current status and future trends, Proc. IEEE 100 (2012) 410–426.

[53] J.C. Ganley, High temperature and pressure alkaline electrolysis, Int. J. Hydrog. Energy 34 (2009) 3604–3611.

[54] A.J. Appleby, G. Crepy, J. Jacquelin, High efficiency water electrolysis in alkaline solution, Int. J. Hydrog. Energy 3 (1978) 21–37.

[55] H. Wendt, H. Hofmann, Ceramic diaphragms for advanced alkaline water electrolysis, J. Appl. Electrochem. 19 (1989) 605–610.

[56] V. Rosa, New materials for water electrolysis diaphragms, Int. J. Hydrog. Energy 20 (1995) 697–700.

[57] W. Hu, A novel cathode for alkaline water electrolysis, Int. J. Hydrog. Energy 22 (1997) 621–623.

[58] C.K. Kjartansdóttir, L.P. Nielsen, P. Møller, Development of durable and efficient electrodes for large-scale alkaline water electrolysis, Int. J. Hydrog. Energy 38 (2013) 8221–8231.

[59] L.A. Diaz, R.E. Coppola, G.C. Abuin, R. Escudero-Cid, D. Herranz, P. Ocón, Alkali-doped polyvinyl alcohol-Polybenzimidazole membranes for alkaline water electrolysis, J. Membr. Sci. 535 (2017) 45–55.

[60] L.A. Diaz, J. Hnát, N. Heredia, M.M. Bruno, F.A. Viva, M. Paidar, H.R. Corti, K. Bouzek, G.C. Abuin, Alkali doped poly (2,5-benzimidazole) membrane for alkaline water electrolysis: characterization and performance, J. Power Sources 312 (2016) 128–136.

[61] R. Brimblecombe, G.F. Swiegers, G.C. Dismukes, S. Spiccia, Sustained water oxidation photocatalysis by a bioinspired manganese cluster, Angew. Chem. Int. Ed. 120 (2008) 7445–7448.

[62] V. Schröder, B. Emonts, H. Janßen, H.P. Schulze, Explosion limits of hydrogen/oxygen mixtures at initial pressures up to 200 bar, Chem. Eng. Technol. 27 (2004) 847–851.

[63] J. Hnát, M. Paidar, J. Schauer, K. Bouzek, Polymer anion-selective membrane for electrolytic water splitting: the impact of a liquid electrolyte composition on the process parameters and long-term stability, Int. J. Hydrog. Energy 39 (2014) 4779–4787.

[64] M.K. Cho, A. Lim, S.Y. Lee, H.-J. Kim, S.J. Yoo, Y.-E. Sung, H.S. Park, J.H. Jang, A review on membranes and catalysts for anion exchange membrane water electrolysis single cells, J. Electrochem. Sci. Technol. 8 (2017) 183–196.

[65] P. Fortin, T. Khoza, X. Cao, S.Y. Martinsen, A.O. Barnett, S. Holdcrofta, High-performance alkaline water electrolysis using AemionTM anion exchange membranes, J. Power Sources 451 (2020), 227814.

[66] A. Carbone, S. Campagna Zignani, I. Gatto, S. Trocino, A.S. Aricò, Assessment of the FAA3-50 polymer electrolyte in combination with a $NiMn_2O_4$ anode catalyst for anion exchange membrane water electrolysis, Int. J. Hydrog. Energy 45 (2020) 9285–9292.

[67] C. Acar, I. Dincer, Comparative assessment of hydrogen production methods from renewable and non-renewable methods, Int. J. Hydrog. Energy 39 (2014) 1–12.

[68] J.R. Varcoe, P. Atanassov, D.R. Dekel, A.M. Herring, M.A. Hickner, P.A. Kohl, A. R. Kucernak, W.E. Mustain, K. Nijmeijer, K. Scott, T. Xu, L. Zhuang, Anion-exchange membranes in electrochemical energy systems, Energy Environ. Sci. 7 (2014) 3135–3191.

[69] M.K. Cho, H.-Y. Park, H.J. Lee, H.-J. Kim, A. Lim, D. Henkensmeier, S.J. Yoo, J. Y. Kim, S.Y. Lee, H.S. Park, J.H. Jang, Alkaline anion exchange membrane water electrolysis: effects of electrolyte feed method and electrode binder content, J. Power Sources 382 (2018) 22–29.

[70] K. Ham, S. Hong, S. Kang, K. Cho, J. Lee, Extensive active-site formation in trirutile $CoSb_2O_6$ by oxygen vacancy for oxygen evolution reaction in anion exchange membrane water splitting, ACS Energy Lett. 6 (2021) 364–370.

[71] X. Cao, D. Novitski, S. Holdcroft, Visualization of hydroxide ion formation upon electrolytic water splitting in an anion exchange membrane, ACS Mater. Lett. 1 (2019) 362–366.

[72] M.K. Cho, H.-Y. Park, S. Choe, S.J. Yoo, J.Y. Kim, H.-J. Kim, D. Henkensmeier, S. Y. Lee, Y.-E. Sung, H.S. Park, J.H. Jang, Factors in electrode fabrication for performance enhancement of anion exchange membrane water electrolysis, J. Power Sources 347 (2017) 283–290.

[73] A.Y. Faid, L. Xie, A.O. Barnett, F. Seland, D. Kirk, S. Sunde, Effect of anion exchange ionomer content on electrode performance in AEM water electrolysis, Int. J. Hydrog. Energy 45 (2020) 28272–28284.

[74] G.-C. Chen, T.H. Wondimu, H.-C. Huang, K.-C. Wang, C.-H. Wang, Microwave-assisted facile synthesis of cobalt iron oxide nanocomposites for oxygen production using alkaline anion exchange membrane water electrolysis, Int. J. Hydrog. Energy 44 (2019) 10174–10181.

[75] E. Cossar, A.O. Barnett, F. Seland, E.A. Baranova, The performance of nickel and nickel-iron catalysts evaluated as anodes in anion exchange membrane water electrolysis, Catalysts 9 (2019) 814.

[76] A.Y. Faid, A.O. Barnett, F. Seland, S. Sunde, NiCu mixed metal oxide catalyst for alkaline hydrogen evolution in anion exchange membrane water electrolysis, Electrochim. Acta 371 (2021), 137837.

[77] D. Aili, M.K. Hansen, R.F. Renzaho, Q. Li, E. Christensen, J.O. Jensen, N. J. Bjerrum, Heterogeneous anion conducting membranes based on linear and crosslinked KOH doped polybenzimidazole for alkaline water electrolysis, J. Membr. Sci. 447 (2013) 424–432.

[78] J.E. Chae, S.Y. Lee, S.J. Yoo, J.Y. Kim, J.H. Jang, H.-Y. Park, H.S. Park, B. Seo, D. Henkensmeier, K.H. Song, H.-J. Kim, Polystyrene-based hydroxide-ion-conducting ionomer: binder characteristics and performance in anion-exchange membrane fuel cells, Polymers 13 (2021) 690.

[79] A.Y. Faid, A.O. Barnett, F. Seland, S. Sunde, Highly active nickel-based catalyst for hydrogen evolution in anion exchange membrane electrolysis, Catalysts 8 (2018) 614.

[80] K.F.L. Hagesteijn, S. Jiang, B.P. Ladewig, A review of the synthesis and characterization of anion exchange membranes, J. Mater. Sci. 53 (2018) 11131–11150.

[81] J. Mahmood, F. Li, S.-M. Jung, M.S. Okyay, I. Ahmad, S.-J. Kim, N. Park, H. Y. Jeong, J.-B. Baek, An efficient and pH-universal ruthenium-based catalyst for the hydrogen evolution reaction, Nat. Nanotechnol. 12 (2017) 441–446.

[82] F. Li, G.-F. Han, H.-J. Noh, J.-P. Jeon, I. Ahmad, S. Chen, C. Yang, Y. Bu, Z. Fu, Y. Lu, J.-B. Baek, Balancing hydrogen adsorption/desorption by orbital modulation for efficient hydrogen evolution catalysis, Nat. Commun. 10 (2019) 4060.

[83] D.H. Kweon, M.S. Okyay, S.-J. Kim, J.-P. Jeon, H.-J. Noh, N. Park, J. Mahmood, J.-B. Baek, Ruthenium anchored on carbon nanotube electrocatalyst for hydrogen production with enhanced Faradaic efficiency, Nat. Commun. 11 (2020) 1278.

[84] C. Li, J.-B. Baek, Recent advances in noble metal (Pt, Ru, and Ir)-based electrocatalysts for efficient hydrogen evolution reaction, ACS Omega 5 (2020) 31–40.

[85] S.-Y. Bae, J. Mahmood, I.-Y. Jeon, J.-B. Baek, Recent advances in ruthenium-based electrocatalysts for the hydrogen evolution reaction, Nanoscale Horiz. 5 (2020) 43–56.

[86] R. Parsons, The rate of electrolytic hydrogen evolution and the heat of adsorption of hydrogen, Trans. Faraday Soc. 54 (1958) 1053–1063.

[87] R. Subbaraman, D. Tripkovic, K.C. Chang, D. Strmcnik, A.P. Paulikas, P. Hirunsit, M. Chan, J. Greeley, V. Stamenkovic, N.M. Markovic, Trends in activity for the water electrolyser reactions on 3d M (Ni, Co, Fe, Mn) hydr(oxy) oxide catalysts, Nat. Mater. 11 (2012) 550–557.

[88] C. Hu, L. Zhang, J. Gong, Recent progress made in the mechanism comprehension and design of electrocatalysts for alkaline water splitting, Energy Environ. Sci. 12 (2019) 2620–2645.

[89] E. Liu, J. Li, L. Jiao, H.T.T. Doan, Z. Liu, Z. Zhao, Y. Huang, K.M. Abraham, S. Mukerjee, Q. Jia, Unifying the hydrogen evolution and oxidation reactions kinetics in base by identifying the catalytic roles of hydroxyl-water-cation adducts, J. Am. Chem. Soc. 141 (2019) 3232–3239.

[90] Y.-C. Cao, X. Wu, K. Scott, A quaternary ammonium grafted poly vinyl benzyl chloride membrane for alkaline anion exchange membrane water electrolysers with no-noble-metal catalysts, Int. J. Hydrog. Energy 37 (2012) 9524–9528.

[91] S.H. Ahn, S.J. Yoo, H.-J. Kim, D. Henkensmeier, S.W. Nam, S.-K. Kim, J.H. Jang, Anion exchange membrane water electrolyzer with an ultra-low loading of Pt-decorated Ni electrocatalyst, Appl. Catal. B Environ. 180 (2016) 674–679.

[92] S.H. Ahn, B.S. Lee, I. Choi, S.J. Yoo, H.J. Kim, E. Cho, D. Henkensmeier, S. W. Nam, S.K. Kim, J.H. Jang, Development of a membrane electrode assembly for alkaline water electrolysis by direct electrodeposition of nickel on carbon papers, Appl. Catal. B Environ. 154 (2014) 197–205.

[93] C.C. Pavel, F. Cecconi, C. Emiliani, S. Santiccioli, A. Scaffidi, S. Catanorchi, M. Comotti, Highly efficient platinum group metal free based membrane-electrode assembly for anion exchange membrane water electrolysis, Angew. Chem. Int. Ed. 53 (2014) 1378–1381.

[94] L. Xiao, S. Zhang, J. Pan, C. Yang, M. He, L. Zhuang, J. Lu, First implementation of alkaline polymer electrolyte water electrolysis working only with pure water, Energy Environ. Sci. 5 (2012) 7869–7871.

[95] X. Ge, Y. He, M.D. Guiver, L. Wu, J. Ran, Z. Yang, T. Xu, Alkaline anion-exchange membranes containing mobile ion shuttles, Adv. Mater. 28 (2016) 3467–3472.

[96] S. Seetharaman, R. Balaji, K. Ramya, K.S. Dhathathreyan, M. Velan, Graphene oxide modified non-noble metal electrode for alkaline anion exchange membrane water electrolyzers, Int. J. Hydrog. Energy 38 (2013) 14934–14942.

[97] G. Zhang, Y.-S. Feng, W.-T. Lu, C.-Y. Wang, Y.-K. Li, X.-Y. Wang, F.-F. Cao, Enhanced catalysis of electrochemical overall water splitting in alkaline media by Fe doping in Ni_3S_2 nanosheet arrays, ACS Catal. 8 (2018) 5431–5441.

[98] C. Li, G. Wang, K. Li, Y. Liu, B. Yuan, Y. Lin, FeNi-based coordination crystal directly serving as efficient oxygen evolution reaction catalyst and its density functional theory insight on the active site change mechanism, ACS Appl. Mater. Interfaces 11 (2019) 20778–20787.

[99] C. Li, Y. Liu, G. Wang, L. Guan, Y. Lin, Binding energy optimization strategy inducing enhanced catalytic performance on MIL-100(FeNi) to catalyze water oxidation directly, ACS Sustain. Chem. Eng. 7 (2019) 7496–7501.

[100] M. Gong, H. Dai, A mini review of NiFe-based materials as highly active oxygen evolution reaction electrocatalysts, Nano Res. 8 (2015) 23–39.

[101] S.C. Zignani, M.L. Faro, S. Trocino, A.S. Aricò, Investigation of NiFe-based catalysts for oxygen evolution in anion-exchange membrane electrolysis, Energies 13 (2020) 1720.

[102] Z. Qiu, C.-W. Tai, G.A. Niklasson, T. Edvinsson, Direct observation of active catalyst surface phases and the effect of dynamic self-optimization in NiFe-layered double hydroxides for alkaline water splitting, Energy Environ. Sci. 12 (2019) 572–581.

[103] H. Koshikawa, H. Murase, T. Hayashi, K. Nakajima, H. Mashiko, S. Shiraishi, Y. Tsuji, Single nanometer-sized NiFe-layered double hydroxides as anode catalyst in anion exchange membrane water electrolysis cell with energy conversion efficiency of 74.7% at 1.0 A cm^{-2}, ACS Catal. 10 (2020) 1886–1893.

[104] D. Xu, M.B. Stevens, M.R. Cosby, S.Z. Oener, A.M. Smith, L.J. Enman, K.E. Ayers, C.B. Capuano, J.N. Renner, N. Danilovic, Y. Li, H. Wang, Q. Zhang, S. W. Boettcher, Earth-abundant oxygen electrocatalysts for alkaline anion-exchange-membrane water electrolysis: effects of catalyst conductivity and comparison with performance in three-electrode cells, ACS Catal. 9 (2019) 7–15.

[105] M.J. Jang, J. Yang, J. Lee, Y.S. Park, J. Jeong, S.M. Park, J.-Y. Jeong, Y. Yin, M.-H. Seo, S.M. Choi, K.H. Lee, Superior performance and stability of anion exchange membrane water electrolysis: pH-controlled copper cobalt oxide nanoparticles for the oxygen evolution reaction, J. Mater. Chem. A 8 (2020) 4290–4299.

[106] S. Kang, K. Ham, J. Lee, Moderate oxophilic CoFe in carbon nanofiber for the oxygen evolution reaction in anion exchange membrane water electrolysis, Electrochim. Acta 353 (2020), 136521.

[107] M.R. Kraglund, M. Carmo, G. Schiller, S.A. Ansar, D. Aili, E. Christensen, J. O. Jensen, Ion-solvating membranes as a new approach towards high rate alkaline electrolyzers, Energy Environ. Sci. 12 (2019) 3313–3318.

[108] S. Kim, S. Yang, D. Kim, Poly(arylene ether ketone) with pendant pyridinium groups for alkaline fuel cell membranes, Int. J. Hydrog. Energy 42 (2017) 12496–12506.

[109] C. Vogel, J. Meier-Haack, Preparation of ion-exchange materials and membranes, Desalination 342 (2014) 156–174.

[110] N. Lee, D.T. Duong, D. Kim, Cyclic ammonium grafted poly (arylene ether ketone) hydroxide ion exchange membranes for alkaline water electrolysis with high chemical stability and cell efficiency, Electrochim. Acta 271 (2018) 150–157.

[111] M.M. Nasef, O. Güvenc, Radiation-grafted copolymers for separation and purification purposes: status, challenges and future directions, Prog. Polym. Sci. 37 (2012) 1597–1656.

[112] A. Marinkas, I. Struźyńska-Piron, Y. Lee, A. Lim, H.S. Park, J.H. Jang, H.-J. Kim, J. Kim, A. Maljusch, O. Conradi, D. Henkensmeier, Anion-conductive membranes based on 2-mesityl-benzimidazolium functionalised poly(2,6-dimethyl-1,4-phenylene oxide) and their use in alkaline water electrolysis, Polymer 145 (2018) 242–251.

[113] S. Miyanishi, T. Yamaguchi, Highly conductive mechanically robust high M_w polyfluorene anion exchange membrane for alkaline fuel cell and water electrolysis application, Polym. Chem. 11 (2020) 3812–3820.

[114] J.S. Olsson, T.H. Pham, P. Jannasch, Poly(arylene piperidinium) Hydroxide ion exchange membranes: synthesis, alkaline stability, and conductivity, Adv. Funct. Mater. 28 (2018), 1702758.

[115] Y.S. Park, J. Yang, J. Lee, M.J. Jang, J. Jeong, W.-S. Choi, Y. Kim, Y. Yin, M. H. Seo, Z. Chen, S.M. Choi, Superior performance of anion exchange membrane water electrolyzer: ensemble of producing oxygen vacancies and controlling mass transfer resistance, Appl. Catal. B Environ. 278 (2020), 119276.

[116] H.J. Park, S.Y. Lee, T.K. Lee, H.-J. Kim, Y.M. Lee, N3-butyl imidazolium-based anion exchange membranes blended with Poly(vinyl alcohol) for alkaline water electrolysis, J. Membr. Sci. 611 (2020), 118355.

[117] L. Zeng, T.S. Zhao, An effective strategy to increase hydroxide-ion conductivity through microphase separation induced by hydrophobic-side chains, J. Power Sources 303 (2016) 354–362.

[118] D.D. Tham, D. Kim, C2 and N3 substituted imidazolium functionalized poly (arylene ether ketone) anion exchange membrane for water electrolysis with improved chemical stability, J. Membr. Sci. 581 (2019) 139–149.

[119] J. Hnát, M. Plevová, J. Žitka, M. Paidar, K. Bouzek, Anion-selective materials with 1,4-diazabicyclo[2.2.2]octane functional groups for advanced alkaline water electrolysis, Electrochim. Acta 248 (2017) 547–555.

[120] G. Yang, J. Hao, J. Cheng, N. Zhang, G. He, F. Zhang, C. Hao, Hydroxide ion transfer in anion exchange membrane: a density functional theory study, Int. J. Hydrog. Energy 41 (2016) 6877–6884.

[121] S. Devaraj, N. Munichandraiah, Effect of crystallographic structure of MnO_2 on its electrochemical capacitance properties, J. Phys. Chem. C 112 (2008) 4406–4417.

[122] S. Chempath, J.M. Boncella, L.R. Pratt, N. Henson, B.S. Pivovar, Structural, electronic, and vibrational properties of amino-adamantane and rimantadine isomers, J. Phys. Chem. C 114 (2010) 11977–11983.

[123] C. Chen, Y.L.S. Tse, G.E. Lindberg, C. Knight, G.A. Voth, Hydroxide solvation and transport in anion exchange membranes, J. Am. Chem. Soc. 138 (2016) 991–1000.

[124] A. Kusoglu, A.Z. Weber, New insights into perfluorinated sulfonic-acid ionomers, Chem. Rev. 117 (2017) 987–1104.

[125] D. Henkensmeier, M. Najibah, C. Harms, J. Žitka, J. Hnát, K. Bouzek, Overview: state-of-the art commercial membranes for anion exchange membrane water electrolysis, J. Electrochem. Energy Convers. Stor. 18 (2021), 024001.

[126] M.R. Hibbs, M.A. Hickner, T.M. Alam, S.K. Mcntyre, C.H. Fujimoto, C. J. Cornelius, Transport properties of hydroxide and proton conducting membranes, Chem. Mater. 20 (2008) 2566–2573.

[127] J. Müller, A. Zhegur, U. Krewer, J.R. Varcoe, D.R. Dekel, Practical ex-situ technique to measure the chemical stability of anion-exchange membranes under conditions simulating the fuel cell environment, ACS Mater. Lett. 2 (2020) 168–173.

[128] J. Parrondo, C.G. Arges, M. Niedzwiecki, E.B. Anderson, K.E. Ayers, V. Ramani, Degradation of anion exchange membranes used for hydrogen production by ultrapure water electrolysis, RSC Adv. 4 (2014) 9875–9879.

[129] C.G. Arges, V. Ramani, Two-dimensional NMR spectroscopy reveals cation-triggered backbone degradation in polysulfone-based anion exchange membranes, Proc. Natl. Acad. Sci. USA 110 (2013) 2490–2495.

[130] M. Tomoi, K. Yamaguchi, R. Ando, Y. Kantake, Y. Aosaki, H. Kubota, Synthesis and thermal stability of novel anion exchange resins with spacer chains, J. Appl. Polym. Sci. 64 (1997) 1161–1167.

[131] M.R. Hibbs, Alkaline stability of poly (phenylene)-based anion exchange membranes with various cations, J. Polym. Sci. Part B Polym. Phys. 51 (2012) 1736–1742.

[132] H. Long, K. Kim, B.S. Pivovar, Hydroxide degradation pathways for substituted trimethylammonium cations: a DFT study, J. Phys. Chem. C 116 (2012) 9419–9426.

[133] Z. Zhang, L. Wu, J. Varcoe, C. Li, A.L. Ong, S. Poynton, T. Xu, Aromatic polyelectrolytes via polyacylation of pre-quaternized monomers for alkaline fuel cells, J. Mater. Chem. A 1 (2013) 2595–2601.

[134] M.G. Marino, K.D. Kreuer, Alkaline stability of quaternary ammonium cations for alkaline fuel cell membranes and ionic liquids, ChemSusChem 8 (2015) 513–523.

[135] T.H. Pham, J.S. Olsson, P. Jannasch, N-spirocyclic quaternary ammonium ionenes for anion-exchange membranes, J. Am. Chem. Soc. 139 (2017) 2888–2891.

[136] J. Ponce-González, D.K. Whelligan, L. Wang, R. Bance-Soualhi, Y. Wang, Y. Peng, H. Peng, D.C. Apperley, H.N. Sarode, T.P. Pandey, A.G. Divekar, S. Seifert, A. M. Herring, L. Zhuang, J.R. Varcoe, High performance aliphatic-heterocyclic benzyl-quaternary ammonium radiation-grafted anion-exchange membranes, Energy Environ. Sci. 9 (2016) 3724–3735.

[137] A. Lim, H.-j Kim, D. Henkensmeier, S.J. Yoo, J.Y. Kim, S.Y. Lee, Y.-E. Sung, J. H. Jang, H.S. Park, A study on electrode fabrication and operation variables affecting the performance of anion exchange membrane water electrolysis, J. Ind. Eng. Chem. 76 (2019) 410–418.

[138] E.N. Komkova, D.F. Stamatialis, H. Strathmann, M. Wessling, Anion-exchange membranes containing diamines: preparation and stability in alkaline solution, J. Membr. Sci. 244 (2004) 25–34.

[139] D. Li, E.J. Park, W. Zhu, Q. Shi, Y. Zhou, H. Tian, Y. Lin, A. Serov, B. Zulevi, E. D. Baca, C. Fujimoto, H.T. Chung, Y.S. Kim, Highly quaternized polystyrene ionomers for high performance anion exchange membrane water electrolysers, Nat. Energy 5 (2020) 378–385.

[140] X. Zhang, Y. Cao, M. Zhang, Y. Wang, H. Tang, N. Li, Olefin metathesis-crosslinked, bulky imidazolium-based anion exchange membranes with excellent base stability and mechanical properties, J. Membr. Sci. 598 (2020), 117793.

[141] A. Amel, N. Gavish, L. Zhu, D.R. Dekel, M.A. Hickner, Y. Ein-Eli, Bicarbonate and chloride anion transport in anion exchange membranes, J. Membr. Sci. 514 (2016) 125–134.

[142] H. Tang, S. Wang, S.P. Jiang, M. Pan, A comparative study of CCM and hot-pressed MEAs for PEM fuel cells, J. Power Sources 170 (2007) 140–144.

[143] X. Chu, Y. Shi, L. Liu, Y. Huang, N. Li, Piperidinium-functionalized anion exchange membranes and their application in alkaline fuel cells and water electrolysis, J. Mater. Chem. A 7 (2019) 7717–7727.

[144] J.A. Elliott, S.J. Paddison, Modelling of morphology and proton transport in PFSA membranes, Phys. Chem. Chem. Phys. 9 (2007) 2602–2618.

[145] S. Vengatesan, S. Santhi, S. Jeevanantham, G. Sozhan, Quaternized poly (styrene-co-vinylbenzyl chloride) anion exchange membranes for alkaline water electrolysers, J. Power Sources 284 (2015) 361–368.
[146] L. Zeng, T.S. Zhao, Integrated inorganic membrane electrode assembly with layered double hydroxides as ionic conductors for anion exchange membrane water electrolysis, Nano Energy 11 (2015) 110–118.
[147] S.A. Grigoriev, A.S. Pushkarev, I.V. Pushkareva, P. Millet, A.S. Belov, V. V. Novikov, I.G. Belaya, Y.Z. Voloshin, Hydrogen production by proton exchange membrane water electrolysis using cobalt and iron hexachloroclathrochelates as efficient hydrogen-evolving electrocatalysts, Int. J. Hydrog. Energy 42 (2017) 27845–27850.
[148] Y. Shao, G. Yin, Z. Wang, Y. Gao, Proton exchange membrane fuel cell from low temperature to high temperature: material challenges, J. Power Sources 167 (2007) 235–242.
[149] H.-Y. Jung, K.-Y. Cho, K.A. Sung, W.-K. Kim, J.-K. Park, The effect of sulfonated poly(ether ether ketone) as an electrode binder for direct methanol fuel cell (DMFC), J. Power Sources 163 (2006) 56–59.
[150] S. Kundu, M.W. Fowler, L.C. Simon, S. Grot, Morphological features (defects) in fuel cell membrane electrode assemblies, J. Power Sources 157 (2006) 650–656.
[151] Y. Leng, G. Chen, A.J. Mendoza, T.B. Tighe, M.A. Hickner, C.Y. Wang, Solid-state water electrolysis with an alkaline membrane, J. Am. Chem. Soc. 134 (2012) 9054–9057.
[152] J. Hnát, M. Plevova, R.A. Tufa, J. Zitka, M. Paidar, K. Bouzek, Development and testing of a novel catalyst-coated membrane with platinum-free catalysts for alkaline water electrolysis, Int. J. Hydrog. Energy 44 (2019) 17493–17504.
[153] X. Wu, K. Scott, A non-precious metal bifunctional oxygen electrode for alkaline anion exchange membrane cells, J. Power Sources 206 (2012) 14–19.
[154] G. Borisov, H. Penchev, K. Maksimova-Dimitrova, F. Ublekov, E. Lefterova, V. Sinigersky, E. Slavcheva, Alkaline water electrolysis facilitated via non-precious monometallic catalysts combined with highly KOH doped polybenzimidazole membrane, Mater. Lett. 240 (2019) 144–146.
[155] V. Vijayakumar, S.Y. Nam, Recent advancements in applications of alkaline anion exchange membranes for polymer electrolyte fuel cells, J. Ind. Eng. Chem. 70 (2019) 70–86.
[156] J.E. Park, S.Y. Kang, S.H. Oh, J.K. Kim, M.S. Lim, C.Y. Ahn, Y.H. Cho, Y.E. Sung, High-performance anion-exchange membrane water electrolysis, Electrochim. Acta 295 (2019) 99–106.
[157] G. Gupta, K. Scott, M. Mamlouk, Performance of polyethylene based radiation grafted anion exchange membrane with polystyrene-b-poly (ethylene/butylene)-b-polystyrene based ionomer using $NiCo_2O_4$ catalyst for water electrolysis, J. Power Sources 375 (2018) 387–396.
[158] X. Wu, K. Scott, A polymethacrylate-based quaternary ammonium OH^- ionomer binder for non-precious metal alkaline anion exchange membrane water electrolysers, J. Power Sources 214 (2012) 124–129.
[159] X. Wu, K. Scott, A Li-doped Co_3O_4 oxygen evolution catalyst for non-precious metal alkaline anion exchange membrane water electrolysers, Int. J. Hydrog. Energy 38 (2013) 3123–3129.
[160] D. Chanda, J. Hnát, T. Bystron, M. Paidar, K. Bouzek, Optimization of synthesis of the nickel-cobalt oxide based anode electrocatalyst and of the related membrane-electrode assembly for alkaline water electrolysis, J. Power Sources 347 (2017) 247–258.
[161] J. Ran, L. Wu, B. Wei, Y. Chen, T. Xu, Simultaneous enhancements of conductivity and stability for anion exchange membranes (AEMs) through precise structure design, Sci. Rep. 4 (2014) 6486.
[162] H. Ishikawa, E. Haryuu, N. Kawasaki, H. Daimon, Development of 70 Mpa differential-pressure water electrolysis stack, Honda RD Tech. Rev. 28 (2016) 86–93.
[163] H. Ito, N. Kawaguchi, S. Someya, T. Munakata, Pressurized operation of anion exchange membrane water electrolysis, Electrochim. Acta 297 (2019) 188–196.
[164] H. Ito, N. Miyazaki, S. Sugiyama, M. Ishida, Y. Nakamura, S. Iwasaki, Y. Hasegawa, A. Nakano, Investigations on electrode configurations for anion exchange membrane electrolysis, J. Appl. Electrochem. 48 (2018) 305–316.
[165] H. Ito, N. Kawaguchi, S. Someya, T. Munakata, N. Miyazaki, M. Ishida, A. Nakano, Experimental investigation of electrolytic solution for anion exchange membrane water electrolysis, Int. J. Hydrog. Energy 43 (2018) 17030–17039.
[166] W. You, E. Padgett, S.N. MacMillan, D.A. Muller, G.W. Coates, Highly conductive and chemically stable alkaline anion exchange membranes via ROMP of trans-cyclooctene derivatives, Proc. Natl. Acad. Sci. USA 116 (2019) 9729–9734.
[167] DOE H2A Analysis, ⟨https://www.hydrogen.energy.gov/h2a_analysis.html/⟩, 2021 (accessed 4 Februry 2021).
[168] National Renewable Energy Laboratory, FY 2021 Site Sustainability Plan, National Renewable Energy Laboratory, Golden, CO, 2021 accessed 4 Februry 2021, https://www.nrel.gov/docs/fy21osti/78706.pdf.
[169] B. James, W. Colella, J. Moton, G. Saur, T. Ramsden, National Renewable Energy Lab. (NREL), Golden, CO, USA 2013, 27 pp, ⟨https://www.hydrogen.energy.gov/pdfs/h2a_pem_electrolysis_case_study_documentation.pdf⟩, accessed 4 February 2021.
[170] R. Abbasi, B.P. Setzler, S. Lin, J. Wang, Y. Zhao, H. Xu, B. Pivovar, B. Tian, X. Chen, G. Wu, Y. Yan, A roadmap to low-cost hydrogen with hydroxide exchange membrane electrolyzers, Adv. Mater. 31 (2019), 1805876.
[171] X.Z. Chen, J. Qi, P. Wang, C. Li, X. Chen, C.H. Liang, Polyvinyl alcohol protected Mo_2C/Mo_2N multicomponent electrocatalysts with controlled morphology for hydrogen evolution reaction in acid and alkaline medium, Electrochim. Acta 273 (2018) 239–247.
[172] C.-W. Tung, Y.-Y. Hsu, Y.-P. Shen, Y. Zheng, T.-S. Chan, H.-S. Sheu, Y.-C. Cheng, H.M. Chen, Reversible adapting layer produces robust single-crystal electrocatalyst for oxygen evolution, Nat. Commun. 6 (2015) 8106.
[173] EU's Funding Programme for Research and Innovation, Horizon 2020, Fuel Cells and Hydrogen Joint Undertaking (FCH JU). Multi-Annual Work Plan 2014–2020 2016, ⟨https://fch.europa.eu/sites/default/files/FCH%202%20JU%20MAWP-%20final%20%28ID%204221004%29.pdf⟩ (accessed: October 2020).
[174] O. Schmidt, A. Gambhir, I. Staffell, A. Hawkes, J. Nelson, S. Few, Future cost and performance of water electrolysis: an expert elicitation study, Int. J. Hydrog. Energy 42 (2017) 30470–30492.
[175] M. Gong, Y. Li, H. Wang, Y. Liang, J.Z. Wu, J. Zhou, J. Wang, T. Regier, F. Wei, H. Dai, An advanced Ni-Fe layered double hydroxide electrocatalyst for water oxidation, J. Am. Chem. Soc. 135 (2013) 8452–8455.
[176] J.O.M. Bockris, T. Otagawa, The electrocatalysis of oxygen evolution on perovskites, J. Electrochem. Soc. 131 (1984) 290–302.
[177] Y.-Y. Ma, Z.-L. Lang, L.-K. Yan, Y.-H. Wang, H. Tan, K. Feng, Y. Xia, J. Zhong, Y. Liu, Z. Kang, Highly efficient hydrogen evolution triggered by a multi-interfacial Ni/WC hybrid electrocatalyst, Y.-G. Li, Energy Environ. Sci. 11 (2018) 2114–2123.
[178] H. Jin, B. Ruqia, Y. Park, H.J. Kim, H.-S. Oh, S.-I. Choi, K. Lee, Nanocatalyst design for long-term operation of proton/anion exchange membrane water electrolysis, Adv. Energy Mater. 11 (2021), 2003188.
[179] Y. Liang, Y. Li, H. Wang, J. Zhou, J. Wang, T. Regier, H. Dai, Co_3O_4 nanocrystals on graphene as a synergistic catalyst for oxygen reduction reaction, Nat. Mater. 10 (2011) 780–786.
[180] M. Faraj, M. Boccia, H. Miller, F. Martini, S. Borsacchi, M. Geppi, A. Pucci, New LDPE based anion-exchange membranes for alkaline solid polymeric electrolyte water electrolysis, Int. J. Hydrog. Energy 37 (2012) 14992–15002.
[181] Y.S. Park, J.H. Lee, M.J. Jang, J. Jeong, S.M. Park, W.-S. Choi, Y. Kim, J. Yang, S. M. Choi, Co_3S_4 nanosheets on Ni foam via electrodeposition with sulfurization as highly active electrocatalysts for anion exchange membrane electrolyzer, Int. J. Hydrog. Energy 45 (2020) 36–45.

Changqing Li is a PhD candidate in the School of Energy and Chemical Engineering, Center for Dimension-Controllable Organic Frameworks, at Ulsan National Institute of Science and Technology (UNIST), South Korea. He received his M.S. degree at Capital Normal University in 2019. His interest focuses on the design of metal-based materials and carbon based materials for electrochemical applications.

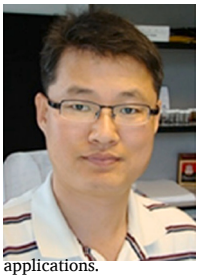

Jong-Beom Baek is a professor and director at the School of Energy and Chemical Engineering, Center for Dimension-Controllable Organic Frameworks, at Ulsan National Institute of Science and Technology (UNIST), South Korea. After receiving his PhD from the University of Akron, USA (Polymer Science, 1998), he joined the Wright-Patterson Air Force Research Laboratory (AFRL). He returned to South Korea to take a position as an assistant professor at Chungbuk National University in 2003, before moving to UNIST in 2008. His current research interests include the synthesis of two-dimensional high-performance polymers and chemical modification of carbon-based materials for multifunctional applications.